

Development of ZIF-67 Derived Electrocatalyst for Oxygen Electrode in Metal Air Batteries



**By
Shahar Yar Khan**

**School of Chemical and Materials Engineering
National University of Science and Technology
2023**

Development of ZIF-67 Derived Electrocatalyst for Oxygen Electrode in Metal Air Batteries



Name: Shahar Yar Khan

Registration No: 00000363354

**This thesis is submitted as a partial fulfillment of the requirements for
the degree of**

MS in Chemical Engineering

Supervisor Name: Dr. Tayyaba Noor

School of Chemical and Materials Engineering (SCME)

National University of Science and Technology (NUST)

H-12, Islamabad, Pakistan

2023



THESIS ACCEPTANCE CERTIFICATE

Certified that final copy of MS Thesis written by **Mr Shahar Yar Khan** (Registration No 00000363354), of School of Chemical & Materials Engineering (SCME) has been vetted by undersigned, found complete in all respects as per NUST Statues/Regulations, is free of plagiarism, errors, and mistakes and is accepted as partial fulfillment for award of MS degree. It is further certified that necessary amendments as pointed out by GEC members of the scholar have also been incorporated in the said Thesis.

Signature: Tayyaba

Name of Supervisor: Dr Tayyaba Noor

Date: 19/7/2023

Signature (HOD): EB

Date: 20/7/23

Signature (Dean/Principal): AK

Date: 20/7/23

CHE-09-2021



Form TH-1

National University of Sciences & Technology (NUST)
MASTER'S THESIS WORK

Formulation of Guidance and Examination Committee (GEC)

Name: Shahar Yar Khan NUST Reg No: 00000363354
 Department: Department of Chemical Engineering Specialization: Master of Science in Chemical Engineering
 Credit Hour Completed: 210 24 CGPA: 3.71 3.75

Course Work Completed

S/No.	Code	Title	Core/Elective	CH	Grade
1.	CHE-843	Separation Processes In Che	Compulsory	3.0	B+
2.	CHE-847	Chemical Kinetics & Reactor Design	Compulsory	3.0	A
3.	RM-898	Research Methodology	Additional	2.0	Q
4.	CHE-815	Nano Catalysis	Elective	3.0	B+
5.	EME-921	Momentum, Heat & Mass Transfer In Chemical Engineering Separation Processes	Compulsory	3.0	B+
6.	CHE-853	Green Process Engineering	Elective	3.0	A
7.	CHE-823	Advance Analytical Techniques	Elective	3.0	A
8.	EME-981	Advance Fuel Technology	Elective	3.0	B+
9.	EME-809	Waste water Treatment & Design	Elective	3.0	A

Date 07-Nov-2022

Student's Signature

Thesis Committee

- Name: Tayyaba Noor (Supervisor)
Department: Department of Chemical Engineering
- Name: Zeeshan Ali (Internal)
Department: Department of Materials Engineering
- Name: Zaib Jahan (Internal)
Department: Department of Chemical Engineering
- Name: Naseem Iqbal (Internal)
Department: Department of Energy Systems Engineering

Signature

Signature

Signature

Signature



Form: TH-04

National University of Sciences & Technology (NUST)

MASTER'S THESIS WORK

We hereby recommend that the dissertation prepared under our supervision by
Regn No & Name: 00000363354 Shahar Yar Khan

Title: Development of ZIF-67 Derived Electrocatalyst for Oxygen Electrode in Metal Air Batteries.

Presented on: 13 Jul 2023 at: 1430 hrs in SCME Seminar Hall

Be accepted in partial fulfillment of the requirements for the award of Master of Science degree
in Chemical Engineering.

Guidance & Examination Committee Members

Name: Dr Naseem Iqbal

Signature: 

Name: Dr Mohsin Saleem

Signature: 


Name: Dr Zaib Jahan


Signature: 

Supervisor's Name: Dr Tayyaba Noor

Signature: 

Dated: 13/7/23


Head of Department
Date 17/7/23


Dean/Principal
Date 18/7/23

School of Chemical & Materials Engineering (SCME)

Dedication

By the grace of Almighty Allah, who is the most Beneficent and the most merciful.

This research is dedicated to my parents, who have always been my source of guidance and support.

To my supervisor who shared his knowledge, gave advice, and encouraged me to fulfill my tasks.

And to all my fellows, with whom I worked and shared good memories.

Acknowledgements

All thanks to Almighty Allah, without His will nothing can happen, who bestowed upon us the ability to think and made us eager to explore the entire universe. Incalculable salutations to the Holy Prophet Hazrat Muhammad (PBUH), the reason for the creation of the cosmos and a source of blessing and knowledge for all humanity.

I am thankful to my research supervisor, Dr. Tayyaba Noor, from the bottom of my heart for her steadfast technical and moral support, as well as for illuminating me with a research vision and pushing me to achieve perfection. Her pursuit of perfection and excellence had served as an inspiration and motivator. Her continual support and encouragement enabled me to reach this difficult goal.

Heartfelt thanks to my committee members and mentor, Dr. Naseem Iqbal, Dr. Mohsin Saleem, and Dr. Zaib Jahan, for mentoring and supporting me throughout my research course. It would not have been possible without their assistance. It would not be possible without Dr. Tayyaba Noor, she helped me by sharing her research expertise and experience.

I am grateful to my seniors, Miss Sadia Altaf and Miss Neelam Zaman, who offered their knowledge of experimental methodologies and motivated me throughout this entire study project. Without a doubt, SCME's support team collaborated with me while I worked on different kinds of equipment.

I am deeply obliged to my siblings and parents for their unending devotion. Thank you for believing in me, wanting the best for me, and motivating me to pursue my dreams. Thank you for your help, wisdom, and encouragement, Najla Javed and Muhammad Mudassar Aslam.

Shahar Yar Khan

Abstract

Scientists and researchers have been pushed to investigate alternate methods of energy conversion and storage by the widespread usage of fossil fuels and the attendant environmental issues. In this endeavor, metal-air batteries, fuel cells, and water splitting have emerged as potentially promising routes to pursue. The high energy density and environmental sustainability of metal-air batteries have led to their emergence as a potentially useful technology for the storage of electrical energy. Nevertheless, the slow oxygen evolution reaction (OER) at the anode continues to be a substantial obstacle, which impedes both the overall performance of metal-air batteries and their applications in real world. ZIF-67 and its composites with reduced graphene oxide (rGO) and manganese (Mn) are the materials that are being investigated for their potential use in the development of an effective electrocatalyst for oxygen electrode in MABs as part of this research.

Using the solvothermal method, we synthesized ZIF-67, 1-5wt% rGO/ZIF-67, and 1-5wt% rGO/Mn ZIF-67. XRD, SEM, Raman, and FTIR characterization techniques were used. We performed cyclic voltammetry, chronopotentiometry, EIS, and LSV tests for electrochemical study.

The overpotential values for ZIF-67 were calculated as 154mV at 10 mAcm⁻². By the addition of rGO, overpotential values were reduced. The optimum addition of rGO was 3wt% as it gave an overpotential value of 136mV 10 mAcm⁻². The addition of 5wt% rGO caused the blockage of active sites. The addition of Mn significantly improved the activity of ZIF-67. 3wt% rGO/Mn ZIF-67 outperformed all the compositions of catalysts being performed in this study, with an overpotential value of 113 mV at 10 mAcm⁻².

According to the findings of the study, the electrocatalyst that was developed from ZIF-67 has superior levels of catalytic activity and stability in comparison to traditional catalysts used in metal-air batteries, particularly for the reaction that involves oxygen evolution. The addition of RGO and Mn to structure of ZIF-67 provides additional active sites for the OER and makes electron transfer more efficient, both of which contribute to

an overall improvement in performance. These findings give important new insights into design and synthesis of effective electrocatalysts for MABs, thereby expanding field of environmentally friendly technologies for the storage of energy.

Table of Contents

.....	
Dedication	i
Acknowledgements	ii
Abstract	iii
Acronym	xi
Chapter 1.....	1
Introduction.....	1
1.1 Background.....	1
1.2 Metal Organic Frameworks (MOFs):.....	2
1.3 Applications of MOF.....	4
1.3.1 Coordination Chemistry.....	4
1.3.2 Hydrogen Storage.....	6
1.3.3 Hydrogen Production.....	7
1.3.4 CO ₂ conversion and storage.....	8
1.4 Oxygen Catalysis.....	10
1.4.1 Oxygen Evolution Reaction.....	10
1.4.2 Oxygen Reduction Reaction.....	13
1.5 Lithium Oxygen Batteries.....	15
1.6 Problem statement.....	17
1.7 Research Objectives.....	17
1.8 Scope of Study.....	17
1.9 Chapter Summary.....	18
Chapter 2.....	19

Literature Review	19
2.1 Literature review	19
Chapter 3	32
Materials and Methods	32
3.1 Raw material	32
3.2 Synthesis of ZIF-67	32
3.3 Synthesis of rGO/ZIF-67	33
3.4 Synthesis of rGO/Mn ZIF-67	34
3.5 Scanning Electron Microscope.....	35
3.6 X-Ray Diffraction	35
3.7 Fourier Transform Infrared	36
3.8 Raman Spectroscopy	36
3.9 Potentiostat	37
3.9.1 Overpotential	37
3.9.2 Tafel Slope.....	37
3.9.3 Stability.....	38
3.9.4 Electrode Characteristics	38
Chapter 4	39
Results and discussion.....	39
4.1 Results and discussion.....	39
4.2 Electrocatalytic Measurements.....	46
4.2.1 Preparation of ZIF 67 Electrode	46

4.2.2 OER.....	46
Conclusion.....	56
Future Recommendations.....	58
References	60

List of Figures

Figure 1: Schematic diagram of application of MOF. Reprinted with permission [37] copyright 2017 Elsevier Inc.	4
Figure 2: Schematic diagram for synthesis of ZIF-67.....	33
Figure 3: Schematic diagram of 1-5wt% rGO/ZIF-67	34
Figure 4: Schematic diagram of 1-5wt% rGO/Mn ZIF-67	35
Figure 5: XRD of ZIF-67, 1wt% rGO/ZIF-67, 3wt% rGO/ZIF-67, 5wt% rGO/ZIF-67.	39
Figure 6: XRD of 1wt% rGO/Mn ZIF-67, 3wt% rGO/Mn ZIF-67, 5wt% rGO/Mn ZIF-67	40
Figure 7: SEM image of a) ZIF-67, b) 1wt% rGO/ZIF-67, c) 3wt% rGO/ZIF-67, d)5wt% rGO/ZIF-67	41
Figure 8: SEM image of a) 1 wt% rGO/Mn ZIF-67 b) 3 wt% rGO/Mn ZIF-67 c) 5 wt% rGO/Mn ZIF-67.....	42
Figure 9: Raman spectroscopy of ZIF-67, 3wt% rGO/ZIF-67, 3wt% rGO/Mn ZIF-67 .	44
Figure 10: FTIR a) ZIF-67, 1wt% rGO/ZIF-67, 3wt% rGO/ZIF-67, 5wt% rGO/ZIF-67 b) 1wt% rGO/Mn ZIF-67, 3wt% rGO/Mn ZIF-67, 5wt% rGO/Mn ZIF-67	45
Figure 11: Cyclic voltammetry plots at 15, 25, 50, 75, 100 mV/s scan rate of a) ZIF-67 b) 1wt% rGO/ZIF-67 c) 3wt% rGO/ZIF-67 d) 5wt% rGO/ZIF-67	47
Figure 12: Cyclic voltammetry plots at 15, 25, 50, 75, 100 mV/s scan rate of a) 1wt% rGO/Mn ZIF-67 b) 3wt% rGO/Mn ZIF-67 c) 5wt% rGO/Mn ZIF-67	48
Figure 13: Combined Cyclic voltammetry plots a) ZIF-67, 1wt% rGO/ZIF-67, 3wt% rGO/ZIF-67, 5wt% rGO/ZIF-67 b) 1wt% rGO/Mn ZIF-67, 3wt% rGO/Mn ZIF-67, 5wt% rGO/Mn ZIF-67	49
Figure 14: LSV plots a) 1wt% rGO/Mn ZIF-67, 3wt% rGO/Mn ZIF-67, 5wt% rGO/Mn ZIF-67 b) ZIF-67, 1wt% rGO/ZIF-67, 3wt% rGO/ZIF-67, 5wt% rGO/ZIF-67	51
Figure 15: Tafel slope a) ZIF-67, 1wt% rGO/ZIF-67, 3wt% rGO/ZIF-67, 5wt% rGO/ZIF-67 b) 1wt% rGO/Mn ZIF-67, 3wt% rGO/Mn ZIF-67, 5wt% rGO/Mn ZIF-67	52

Figure 16: EIS plots a) 1wt% rGO/Mn ZIF-67, 3wt% rGO/Mn ZIF-67, 5wt% rGO/Mn ZIF-67 b) ZIF-67, 1wt% rGO/ZIF-67, 3wt% rGO/ZIF-67, 5wt% rGO/ZIF-67 53

Figure 17: Chronopotentiometry a) 1wt% rGO/Mn ZIF-67, 3wt% rGO/Mn ZIF-67, 5wt% rGO/Mn ZIF-67 b) ZIF-67, 1wt% rGO/ZIF-67, 3wt% rGO/ZIF-67, 5wt% rGO/ZIF-67 55

List of Tables

Table 1: ZIF-67 reported catalytic performance values in literature.	25
Table 2: Energy Dispersive X-Ray Spectroscopy	42
Table 3: Energy Dispersive X-Ray Spectroscopy	43
Table 4: R_u , C_f , and R_{ct} values of synthesized catalysts in this study	54

Acronym

MOF	Metal Organic Framework
FTIR	Fourier transform infrared spectroscopy
MABs	Metal Air Batteries
SEM	Scanning Electron Microscope
EDX	Energy-dispersive-Xray spectroscopy
GCE	Glassy Carbon Electrode
NF	Ni Foam

Chapter 1

Introduction

1.1 Background

In last few decades, there has been a rapid and continuous growth in the amount of energy that is consumed all over the world, and analysts anticipate that this trend will continue until the year 2040. In the past, analysts hypothesized that the amount of energy consumed on a global scale in the 2010s would amount to 524 quadrillion Btu. It is expected that this number will increase to 630 quadrillion Btu in 2020s and by the 2040s it reaches 820 quadrillion Btu [1-3]. As of right now, fossil fuels are responsible for eighty percent of world's consumable energy supply, which has led to a catastrophic and urgent energy crisis as well as global warming. Because of these worries, scientists are motivated to include renewable energy sources into our day-to-day activities. Some examples of such sources include solar power, hydroelectricity, wind energy, and fuel cells [4]. It is essential to have energy conversion and storage devices that are both effective and capable in order to make use of renewable energy sources. This will allow for balancing of energy demand throughout the day and the effective management of the generation intermittent fluctuations or sudden surges [5]. Researchers are making efforts to reduce carbon emissions around the world while also profiting from the conversion of CO₂ and capturing potential sources of renewable energy.

Electrochemical energy conversion and storage methods such as water electrolysis, fuel cells, and MABs rely heavily on two primary reactions of oxygen evolution (OER) and oxygen reduction (ORR). These reactions play critical part in processes of these technologies. These reactions are absolutely necessary in order to enable energy processes in these technologies that are efficient and sustainable [6, 7]. The stability and activity of electrocatalysts toward OER and ORR are essential characteristics that have significant impact on performance of electrochemical application. It is essential to achieve high values in both stability and activity to improve efficacy and efficiency of these processes in variety of electrochemical systems [8]. In these kinds of applications, noble metals are often the most effective electrocatalysts to use. Nanocomposites

based on platinum (Pt) are thought to be effective electrocatalyst for ORR that are currently available for purchase on the commercial market. In spite of this, the OER process makes extensive use of valuable nanocomposites that are based on ruthenium (Ru) and iridium (Ir) [9]. However, there are number of substantial obstacles that need to be overcome before these noble metal-based oxygen electrocatalysts can become widely used. These challenges include the insufficient stability of these materials, the high costs, and the limited availability of these resources. These features make their practical application more difficult and highlight the necessity of the research and development of alternative electrocatalysts that are more stable, cost-effective, and efficient in oxygen electrocatalysis [10, 11]. As a consequence of this, it is of the utmost need to provide alternatives that are both highly effective and long-lasting at an affordable price, preferably with the capacity to serve both the OER and the ORR. Over the course of the past ten years, a wide variety of alternative material, such as nanocarbons, have been produced [12], metal oxides [13], nitrides/carbides [14, 15], have been found to be electroactive towards oxygen's corresponding electrochemical processes [16, 17]. It has been demonstrated that nanocarbons exhibit catalytic stability and activity, which holds great promise [18], catalytic characteristics are improved further by introducing heteroatoms like sulfur, nitrogen, and boron, as well as by altering the geometric and electrical structures of the materials. This can be done in a number of different ways [19]. A number of different Nitrogen doped graphitic nanocarbons, such as graphene, carbon nanotubes (CNTs), and mesoporous carbons have been recognized as having capability of functioning as viable alternatives to platinum group metals (Pt catalysts) [19, 20]. It is believed that the altered carbon flaws and electrical structure generated by foreign heteroatoms are responsible for the increased performance [21]. However, only a few articles have shown that nanocarbons have outstanding durability and activity comparable to Pt/C catalysts [22].

1.2 Metal Organic Frameworks (MOFs):

The development of the utilized materials is critical to the implementation of these advanced applications [23, 24]. The study of metal-organic frameworks, often known as MOFs, has recently considered to be research areas in fields of chemistry and materials, as demonstrated by substantial number of publications in some of most prestigious journals in the field [25]. In general, MOFs can be easily designed and manufactured by assembling various organic ligands and metal

ions/clusters. Synchrotron, neutron diffraction, and/or X-ray, techniques can be used to characterize their framework structures [26]. Due to the highly ordered structures, changeable pore size, ultrahigh porosity, and crystalline nature of MOFs, these materials have been put to good use in the energy conversion and gas capture applications [25]. In addition, by capitalizing on the synergistic effects of functional units, the strategic combination of MOFs with other functional material such as graphene or semiconductors has the potential to produce advanced composites that have superior performance in comparison to performance of individual components. Graphene and semiconductors are two examples of functional materials. This could be the case if the MOFs are combined with other functional materials [27]. In addition, nanostructured MOFs have amount of research as potential precursors for production of wide variety of nanomaterials, including those based on metals as well as those based on carbon and featuring regular porous architectures (for example, phosphides, carbides, oxides, and chalcogenides) [28]. The development of MOF derivatives, which demonstrates the benefits brought about by these materials, is an illustration of how MOF-based materials can be utilized in modifying components and improving structures. Because carbon and nitrogen molecules are so abundant, zeolitic imidazolate frameworks (ZIFs) are an excellent candidate for usage as a precursor for nanocarbon electrocatalysts. ZIFs are a subclass of MOFs [29, 30]. In the N-doped carbon compounds, nitrogen species engage in chemical exchanges with the metal nanoparticles; play the role of heteroatoms [31]. These N-doped nanocarbons have the potential to be useful electrocatalysts for ORR and OER. Nanocomposites generated from MOFs have a low graphitic degree and primarily microporous structures [32] there are some variables that are regarded to be deleterious to the transit of ions and electrons. Despite the fact that a great number of metal oxides and nanocarbons produced from MOFs have been the subject of intensive research as possible electrocatalysts [33, 34], the vast majority of them have an insufficient amount of electrochemical activity. In addition, utilization of MOFs as only precursor for synthesis of NCNTs structures reported infrequently. This is because the usage of MOFs as the only precursor has proved difficult [35]. Zn-Fe-ZIFs pyrolysis resulted in fabricating NCNTs, as demonstrated by Yang et al. Dicyandiamide (DCDA) is used in the creation of these NCNTs as both an inducer of additional N sources and the graphitic structure, and the NCNTs that are produced in this manner do not have any secondary microstructure [36].

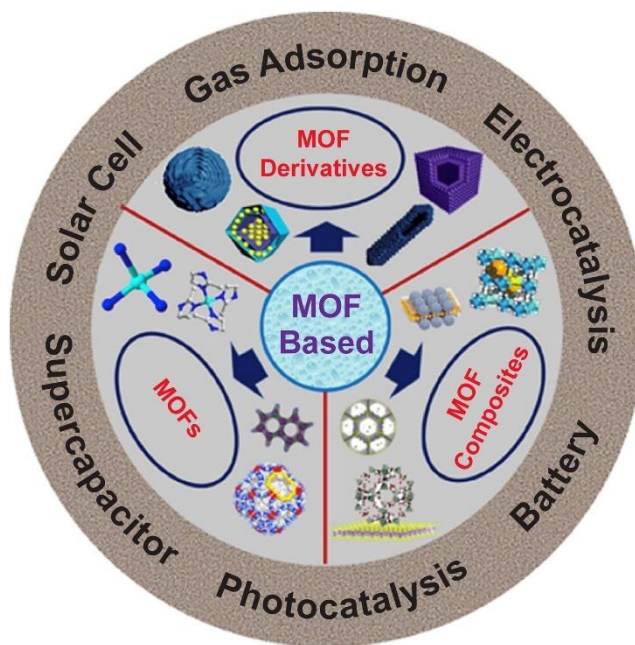


Figure 1: Schematic diagram of application of MOF. Reprinted with permission [37] copyright 2017 Elsevier Inc.

1.3 Applications of MOF

1.3.1 Coordination Chemistry

In the fields of chemistry and material science, MOFs, structured by coordination of in-organic clusters/nodes with organic ligands [37]. Coordination polymers and organic-inorganic hybrids are two subtypes of MOFs that may be distinguished based on their structural differences from a chemical and material science standpoint. Before 1995, each of these kinds emerged through separate evolutionary processes. Yaghi first presented MOF's concept in 1995, elaborated on characteristic of their frameworks as form of porous matrix. MOF's organic linkers are often polytopic or ditopic organic carboxylates or multi nitrogen compound (picolinic acid, and benzenecarboxylate). In these organic linkers, nitrogen and oxygen coordination are the primary mechanisms of coordination [38]. Coordination connection between organic linkers and clusters or metal ions is not only significantly more potent than the hydrogen bonding interaction, but it also demonstrates a larger degree of directionality than other weak interactions (such as the p-p stacking interaction) [39]. MOFs consists of 2 distinct building blocks; hence, their concomitant physicochemical property and structures (such as metal-ligand interactions, crystallinity, porosity) may be easily regulated by making the appropriate choice of organic linkers and metal center. The

fact that MOFs are often made up of two distinct kinds of building units makes this outcome conceivable. MOFs belong to a distinct category of materials because of their one-of-a-kind characteristic, which gives them range of geometries, sizes, functionalities to choose from. In addition, compared with other types of porous materials, MOFs with permanent porosity exhibit a greater degree of variety and multiplicity than any of the other materials. More than 20,000 distinct MOFs have been synthesised and researched up to this point in time. Additionally, MOF's surface area could be customized to be anywhere between 1,000 and 10,000 m^2g^{-1} , values are substantially larger than surface areas of previous porous materials (zeolite, carbon). MOFs are good candidates for the storage and catalysis of gases because of their characteristics, which are described above. On the other hand, MOFs have been shown to be useful precursors in the manufacturing of a wide array of advanced materials [40]. MOF's conversion into metal or carbon-based porous materials is stimulated by porous characteristic, also presence of attractive components, such as diversity of metal ions, organic linkers or clusters. After undergoing heat treatment in the presence of an inert atmosphere, common organic linkers with stiff aromatic rings, such as 1,4-benzenedicarboxylate and benzene-1,3,5-tricarboxylate, have the potential to create a significant yield of carbon. In the meantime, metal ions encased in organic linkers within the MOFs have the potential to undergo a carbon-based thermal reduction process, which would result in the formation of metallic composites. Even if the pores that are created between metal ions, organic linkers in them are altered throughout the process of thermal treatment, the porosity of the product may often be maintained to an acceptable degree. This is because organic linkers and metal ions create pores in parent MOFs. Carbon with pores or carbon-metal composites generated from MOFs may be produced because of carbonization of suitable MOFs, without or with addition of carbon precursors. It is possible that the execution of this method will result in the production of carbon materials generated from MOFs. In addition to providing a variety of nanostructures, MOFs and compounds formed from MOFs have the ability to be selectively modified by heteroatoms. Doping heteroatoms into the ligand prior to calcination and mixing the ligand with heteroatom-containing units during the calcination process are the two most popular approaches of achieving this objective [41, 42]. These modified MOFs not only significantly broaden the use of materials based on MOFs but also significantly compensate for the pure MOFs with standard coordination modes.

1.3.2 Hydrogen Storage

The ability of MOFs to absorb and store gases can be deduced from their definitions. Both the structural optimization of MOFs and the evaluation of their potential to store hydrogen have received a substantial amount of attention and effort. The hydrogen initiative programme was issued by the Department of Energy (DOE) in 2002. This initiative gave a significant boost to the investigation into the storage of hydrogen using materials based on MOFs and pushed into new stage of research. This programme was issued by the former President of the United States, George W. Bush. Since Yaghi reported in 2003 that MOF-5 had the ability to store hydrogen. A significant number of MOFs have been constructed and designed over the course of many years, which has resulted in the development of hundreds of unique structures, exclusively for the purpose of storage of hydrogen. These MOFs have been developed and built specifically for the goal of storing hydrogen [43]. MOFs have an excellent capacity for the gravimetric storage of hydrogen due to extraordinarily high pore volume, surface area, also their low density. At 77 Kelvin and 80 bar, the well-known material MOF-210 holds the record for greatest H₂ gravimetric absorption. This was measured at 17.6 weight percent. This performance is superior to that of zeolite- and carbon-based materials in a significant way [44]. The parameters for hydrogen (H₂) storage that have been established by the DOE include an energy capacity of 5.5 wt% H₂ uptake on mass basis and volume capacity of 40 g L⁻¹ below 100 bar, all while functioning at temperatures that are higher than 233 K. Both of these requirements must be met while the system is under pressure. Despite setting a new record, MOF-210 has not been able to meet these targets despite setting the greatest record possible. Even though there has been steady progress made in the technology utilized for the structural and design optimization of MOFs, it still appears to be a difficult task to accomplish the objective that has been set. It is possible that H₂ storage adsorption force is mostly based on weak van-der-Waals interaction, when operation temperature is increased it becomes weaker. If this is the case, then this could be an explanation for the phenomenon. The incorporation of a large number of adsorption sites into MOF has been one approach that researchers have taken in an effort to address this issue and find a solution. This has allowed them to strengthen interactions between MOFs and hydrogen molecules, which can be seen as an increase in the isosteric heat [45].

1.3.3 Hydrogen Production

Not only can materials based on MOFs participate in the storage of hydrogen, but they also play role in process of photocatalytic water splitting. Hydrogen can be stored in MOF-based materials. Water splits into molecules consisting of oxygen and hydrogen, resulting in a direct transfer from energy of sun to chemical reaction's energy. The process of photocatalytic hydrogen evolution requires the presence of two fundamental functional units: a photosensitizer, which is responsible for the collection of solar energy; co-catalyst, which is responsible for evolution of hydrogen by making use of the electrons acquired from the photosensitizer [27]. Because MOFs are porous, they provide a platform that may be used to incorporate catalytic active sites and light-harvesting units into the matrix. This can be done either through conscious direct synthesis tactics or through post-synthetic methods. A wide variety of MOFs, some of which include functionalized components, have been successfully synthesized and incorporated into photocatalytic hydrogen evolution processes up till this day. The turnover numbers (TONs) can get as high as 7,000, which is equivalent to the numbers for some other metal complexes, the hybrids of those materials, and semiconductors [2].

It is possible to incorporate light-absorbing chromophores into the ligands of MOFs. Examples of such chromophores include 2-aminoterephthalate, Ir/Ru-based complexes, porphyrin units and others. This method not only improves the efficiency with which light energy is captured, but it also encourages the effective separation of charge throughout the process of energy conversion. As a result, MOF can be transformed into good photosensitizers for use in the process of photocatalytic oxidation. As an illustration, iridium complexes that are capable of absorbing light have been integrated into zirconium-based MOF by Wang et al. [46]. It is necessary to load platinum (Pt) nano-particles into pores of the MOF so that they can perform function of a co-catalyst. Developed Pt@MOF hybrid has ability, when stimulated by visible light, to carry out photocatalytic hydrogen evolution in an effective manner. In comparison to systems that are same in composition throughout, this results in a threefold increase in TON, which can reach a maximum of 7,000. In a separate set of tests, the Ru complex was introduced into MOFs so that they could carry out efficient HER reactions when stimulated by visible light [47]. In addition, catalytic sites in forms of coordination unsaturated metals site or metal-oxo clusters can be introduced into MOF using insertion. This makes it possible for MOFs to act as bifunctional

catalysts, serving both as co-catalysts and as photosensitizers. Zhou et al. [48] presented his findings using a post-synthetic method, implanted platinum complexes into the MOF-253 matrix. MOF-253-Pt, in its as-prepared state, can not only gather light from the sun but also function for the HER as active sites. The hydrogen evolution activity of MOF-253-Pt was boosted by a factor of five when compared to that of its parent molecule, MOF-253. These results were obtained using the same reaction conditions as before. By using extended EXAFS, researchers were able to observe a brief Pt-Pt contact in MOF-253-Pt, which contributed to the catalytic performance of catalyst.

MOFs that already contain active sites have the potential to create hydrogen through photocatalytic processes if they are combine with additional light harvester. One recent investigation, which was carried out by Yuan et al. [49] utilized dye Erythrosin B (ErB) in order to sensitise UiO-66 octahedrons for the purpose of photocatalytic hydrogen production. These octahedrons are formed from Zr metal nodes and terephthalic acid ligands. Both MOFs and ErB include benzene rings, one may reasonably anticipate that there will be substantial van-der-Waals interaction and stacking between dyes and MOF. This interaction has been shown to promote effective electron transport in photocatalytic dye-sensitized system. Conduction band potential of UiO-66 is lower than molecular unoccupied orbital lowest potential of ErB, (-0.9V) vs conventional hydrogen electrode (NHE), transfer of electron from photo-excited dye ErB to sites of UiO-66 is thermodynamically favorable. Because of this, it is possible to produce hydrogen. In addition, the photocatalytic activity directed toward the HER was analyzed, and the findings revealed that the MOF incorporation into hybrid system led to an improvement that was about seven times greater. This was determined by comparing the results of the two methods.

1.3.4 CO₂ conversion and storage

In the 21st century, one of the most significant challenges that humanity must overcome is figuring out how to cut down on the quantity of CO₂ that is released into atmosphere by human activities. CO₂ accumulation in atmosphere is fundamental cause of a wide variety of environmental problems, one of which is the acidity of the ocean, which contributes to the issue of global warming. Time has been put into research and development of new materials for collection, storage, conversion of CO₂ that is derived from process streams.

Process of removing carbon dioxide from exhaust gases, which are mostly constituted of N₂ and CO₂, is an essential one that has garnered a lot of attention all around the world. MOFs are considered to be potential candidates for the capture and separation of CO₂ due to their tailorable pore surface and customizable framework [50]. Solid adsorbent selectivity towards CO₂ relative to N₂ and capacity for CO₂ adsorption, both of which are largely reliant on that adsorbent's binding affinity with CO₂, constitute the basis for the evaluation of the solid. The selectivity of a solid adsorbent towards CO₂ relative to N₂ is measured in terms of the selectivity of the adsorbent toward CO₂. It has been found that increasing affinity between CO₂ and MOFs can result in increase in adsorption capacity. This has been accomplished through the development of a variety of methods for pore surface modification. Among these, it has been demonstrated that the effective implantation of alkylamine group or unsaturated metal sites is possible. At a temperature of 296 degrees Kelvin, the MOF-74-Mg, which has metal sites that are unsaturated, has been shown to have the highest CO₂ adsorption capacity ever recorded. It is 23.6 wt.% at 0.1 atm, and it is 35.2 wt.% at 1 atm [51]. However, alkylamine groups give a strong contact with CO₂; weakly interact with N₂, that greatly boost selectivity of CO₂/N₂ of alkylamine MOFs. The alkylamine groups have a strong contact with CO₂, whereas their interaction with N₂ is very weak [50]. Other features, humidity tolerance, are relevant for commercial applications; however, they received far less attention than the binding affinity adsorption enthalpy parameter. This is even though these qualities are significant for practical applications. Although both parameters are significant, this result was obtained. A monodentate-hydroxide pore structure was described by Liao et al. [42] as having ultrahigh capacity of adsorption (9.1 mmol.cm⁻³ at 1 bar and 298 K), adsorption affinity of CO₂ (124 kJ mol⁻¹), and selectivity value of 26 for CO₂/N₂ (298 K). Outstanding performance could be attributed to adsorption and desorption processes caused by the reversible synthesis and deconstruction of bicarbonate that occurs during these activities. Monodentate-hydroxide modified pore surface interacts with CO₂ molecules thanks to the good bonding affinity that exists between the two. This MOF CO₂ capture shows best performance that has been reported. It did this by capturing 13.4 wt.% CO₂ from simulated flue gases (CO₂ pressure at 313 K is 0.10-0.15 bar) at high value of humidity (82%) and being able to quickly release CO₂ under moderate regeneration conditions (N₂purge at 358 K).

Problem described earlier could be remedied by converting carbon dioxide into fuels like carbon monoxide (CO) or methane (CH₄), which would concurrently provide a practical answer to the problem of energy conversion, in other words, the creation of a system for the consumption of energy that does not result in emission of CO₂ [52]. Technologies such as photocatalytic and electrochemical reductions of carbon dioxide would offer enormous benefits to the domains of environmental protection and energy production. Photocatalytic CO₂ reduction is accomplished by making use of the sun's energy to break down the CO₂ molecule, whereas electrocatalytic CO₂ reduction involves electrical energy transformation into value added carbon compounds [27]. Photocatalysis appears to be a more perfect method to tackle world's environmental and energy concerns due to huge supply of solar energy. This is in comparison to electrocatalytic CO₂ reduction. However, the photocatalytic effectiveness of the currently available catalysts is not even close to being sufficient. This is primarily due to the fact that there are not many active sites, there is a low surface area, and electron hole pairs (photogenerated) recombine very quickly.

1.4 Oxygen Catalysis

The ORR and OER are at the heart of a number of different devices that convert energy, such as MABs, fuel cells, water splitting. Effectiveness of these reactions (energy conversion) is substantially limited as a direct result of the slow oxygen involved species reaction kinetics. In order to overcome the energy barrier, effective catalysts are required. Throughout the course of the previous few decades, for these processes electrocatalysts mostly based on precious metal (iridium, platinum, palladium, ruthenium). Large-scale commercial implementations of these technologies have been significantly hampered, however, by their restricted availability and high cost, in addition to their poor stability under working conditions.

1.4.1 Oxygen Evolution Reaction

A sluggish reaction kinetics is experienced by a process involving four electrons that is part of the OER. As a result, high-performance catalysts are essential components that must be present to bring down the overpotential and speed up the OER. Unreasonably high pricing and restricted availability of most effective OER catalysts (noble metal oxide), such as RuO₂ and IrO₂, are a barrier to their commercialization, as these catalysts are essential to the production of OER. Therefore, it is of the utmost importance to rapidly create OER catalysts for energy conversion

that are both highly active and inexpensive. MOFs that have high surface area provide for suitable amount of catalyst electrolyte contact area, and it has been hypothesized that these MOFs are appropriate supports for loading non-noble catalysts towards OER. Co-WOC-1, for instance exhibits exceptional electrocatalytic activity toward the OER when it is put in an alkaline solution [53]. When it comes to this catalyst, mononuclear moieties of $[\text{Co}(\text{H}_2\text{O})_4(\text{DMF})_2]^{2+}$ (DMF = dimethylformamide) are trapped in 3D framework pore. These pores operate for OER as active sites. In alkaline medium, the fact that the Co-WOC-1 has low overpotential (390 mV vs NHE), low Tafel slope (128 mV dec⁻¹) and high TOF (0.05 s⁻¹) reveals that it can be used for OER as effective electrocatalyst.

OER electrocatalysts made from MOFs with heteroatoms doped into nano-carbon materials are another promising material. These electrocatalyst are generated from MOFs. NCNTF catalyst produced through the process of annealing at 700 degrees Celsius ZIF-67 in mixed environment consisting of argon and hydrogen. This catalyst demonstrates outstanding electrocatalytic OER performance with 93 mV dec⁻¹ (Tafel slope), which is a lower value in comparison to the Pt/C electrode, which was 118 mV dec⁻¹ [54]. When compared to standard commercial Pt/C electrode, the NCNTF catalyst for OER has a longer lifespan when operating under the same conditions. Even when all of the conditions are the same, this is still the case. Both the hollow nanostructure and the one-of-a-kind components, which are made up of Co nanoparticles wrapped in layers of carbon shell and crystalline NCNTs, are responsible for the excellent activity of the material. Another remarkable ZIF-67-derived composite has been described by Aijaz et al. [55] This composite is formed by Co@Co₃O₄ nano particles embedding in N-doped carbon-nanotube(CNT)-grafted carbon polyhedral; composite was found to exhibit remarkable properties. After experiencing reductive carbonization (H₂ atmosphere), this newly produced hybrid is then put through a controlled oxidation to finish off the synthesis process. This low-cost catalyst is widely regarded as most effective electrocatalyst due to its ability to generate a reversible overvoltage that is much lower than 0.85 volts (measured against RHE) between ORR and the OER.

There has been a shift in scientific community toward the practice of directly growing; there is no requirement for a binder when using electroactive material on conductive substrate because they operate as catalyst on their own, reach greater levels of electrical conductivity and catalytic

performance. This approach aims to achieve higher levels of catalytic performance and electrical conductivity by eliminating need for binder materials. MOF-engaged approaches, which can be used in a variety of different ways, makes it easier for this trend which develop a range of direct catalysts (integrated electrodes). This is because these methods can be employed in a number of different ways. As an illustration, Ma et al. [56] a method that has been proposed for directly producing catalytically active arrays on conductive matrices. These arrays can subsequently be used as efficient electrodes in electrochemical applications involving OER. This method can be employed, for instance, in electrochemical OER applications. Pyrolysis of MOF precursor (Cotriphenylene-dicarboxylate) was used to make $\text{Co}_3\text{O}_4\text{-C}$ porous nanowire arrays, also known as $\text{Co}_3\text{O}_4\text{-NA}$ for short. The $\text{Co}_3\text{O}_4\text{-NA}$ that was grown on a Cu foil, which is denoted as $\text{Co}_3\text{O}_4\text{-NA/Cu}$, has been directly inserted as working electrode in an alkaline electrolyte in order to boost the OER. A sharp onset potential is produced by the $\text{Co}_3\text{O}_4\text{-NA/Cu}$ electrode at 1.47 V (against RHE), which is a somewhat bigger value than that produced by the IrO_2/C (1.45 V). For achieving current density 10 mA cm^{-2} with either IrO_2/C or the $\text{Co}_3\text{O}_4\text{-NA/Cu}$ electrodes, an operating potential of 1.54 or 1.52 V is required, respectively. The value of Tafel slope for $\text{Co}_3\text{O}_4\text{-NA/Cu}$ electrocatalyst is only 70 mVdec^{-1} , which is significantly less than the IrO_2/C electrocatalyst, which is 97 mVdec^{-1} . During the OER process, having tight gaps between the nanowire arrays is anticipated to be beneficial to mass transfer as well as electrolyte diffusion. Additionally, the close and direct contact that exists between the conductive current collectors and the nanowires has the potential to significantly improve the electrocatalyst's electrical conductivity as well as its durability.

In addition to metal oxides and hybrids of carbon and metal oxides, MOFs could be used as precursors for development of a variety of derivative with rich chemistry that are used to increase the performance of OER. These derivatives are used to improve the efficiency of OER. For instance, metal (such as manganese, cobalt, and nickel) phosphides with a range of various topologies produced from MOF and used as exceptionally for OER as efficient electrocatalysts. In order to synthesize nickel phosphide with plate-like structure, a Ni-based MOFs, also known as Prussian blue analog [PBA] was utilized as precursor in a phosphatizing reaction [57]. In comparison to nickel hydroxide and nickel oxide porous nanoplates, the OER activity of Ni

phosphide porous nanoplates with mixed phases of Ni₂P and Ni₅P₄ has been shown to be superior in the findings of subsequent research. In addition, this porous catalyst displays advantages over a range of other non-noble metal-based catalysts described in literature. In addition to monometal phosphides, carbon-incorporated Ni-Co mixed-metal phosphide nanoboxes that were generated from ZIF-67 can also be derived. These nanoboxes have been designated as NiCoP/C [58]. The overpotential that is necessary for nanoboxes of NiCoP/C is 330 mV, which is significantly less than the overpotentials that are necessary for NiCoP nanoboxes (370 mV) and the Nickel-Cobalt LDH nanoboxes (420 mV). This overpotential is lower than the overpotential that is necessary for the NiCoP nanoboxes to function properly, and its performance is equivalent to that of a large number of other metal-phosphide-based catalysts. This synthetic technique was also extended by Guan et al. in order to facilitate the creation of extremely complicated multi-shelled mixed-metal oxy-phosphide particles [59]. They begin by producing seven-layered Mn-Co oxide particle by exposing Mn-Co coordination polymer spheres to thermal oxidation process. The particles of Mn-Co-oxide are put through a phosphidation treatment after this stage. This treatment leads to the creation of multi-shelled Mn-Co oxy-phosphide particles without inflicting significant structural damage. It is important to note that this approach can be used to generate a variety of various multi-shelled metal oxy-phosphide particle with compositions that can be altered. Overpotentials of around 420 and 370 mV are required for oxide of Mn-Co particle and Mn-Co oxyphosphide, respectively, to achieve current density of 10 mA cm⁻². On other hand, the activated Mn-Co oxyphosphide particles exhibit remarkable activity with regard to OER. They can accomplish this by delivering a current density of 10 mA cm⁻² at an overpotential that is substantially lower than 320 mV. In 1.0 M KOH solution, this value is comparable to that of a large number of other phosphide-based catalyst, such as IrO₂ (338 mV) and RuO₂ (366 mV). These multi-shelled Mn-Co oxyphosphide particles' intricate structure and composition may be responsible for their improved performance. Additionally, the cobalt phosphide may become more conductive and develop new active sites because of the addition of O²⁻ anions and Mn²⁺ cations.

1.4.2 Oxygen Reduction Reaction

In fuel cell, at cathode ORR takes place and mostly follows two pathway: (1) 4-electron pathway that converts oxygen to water directly, and (2) 2-electron pathway that converts oxygen to

hydrogen peroxide. The 2-electron pathway results in the creation of intermediate species of H_2O_2 , which lowers the catalytic activity, hence in theory 4-electron pathway is favored for ORR [60]. Now, most effective catalytic performance with regard to the ORR may be shown in nanomaterials based on platinum. However, their extensive uses are hampered in fuel cells by extremely high cost of such components as well as the extreme scarcity of the components. In the course of the last several decades, large amount of time and resources has been devoted in discovery and development of non-noble metal catalyst alternatives as potential replacements for the traditional catalysts that use noble metals. Along with a high level of surface atom exposure from the catalyst, the necessary catalysts should be easy for O_2 molecules to reach.

MOFs make it feasible to develop sophisticated matrices that have a surface area and active metal site that have been implanted into them. In theory, the framework's porosity assures that the O_2 reactant will have easy access, and metal active sites will serve as foundation for catalytic reaction. There hasn't been a lot of study done on pure MOFs for use in ORR applications because they have a relatively low electron conductivity and aren't very stable in aqueous solutions. Consequently, the development of MOF-derived hybrids with an adequate number of active centers and compositions that are desirable appears to be an elegant solution for addressing the difficulties. Notably, fabrication of carbon matrices heteroatom-doped (CMHD) from MOF-engaged carbonization approach has also been universally regarded as viable means to break carbonaceous matrix' electroneutrality, which results in enhanced conversion and adsorption sites. This is because preparation of the CMHD from the MOF-engaged carbonization process produces increased conversion and adsorption sites. A dual-MOF confined-pyrolysis technique has been developed by Guan et al. [61] in order to produce a $Fe_3C@N-CNT$ assembly that can function as an efficient ORR electrocatalyst. The integration of a MIL-88B nanorods into a MOF host ZIF-8 polyhedron in the capacity of a co-precursor guarantees a confined-pyrolysis process for the aggregation-free synthesis of extremely small Fe_3C nanocrystallite-embedded N-CNTs. The as-prepared $Fe_3C@N-CNT$ assembly has outstanding electrocatalytic activity for ORR in alkaline electrolyte. The amazing activity of these Fe_3C nano-crystallites can be explained by their diminutive size, in addition to the porous and robust N-doped carbon matrix. In an oxygen-saturated solution, it is possible to make out a distinct cathodic peak at a potential of 0.83 volts

relative to RHE. The accompanying Koutecky-Levich graphs demonstrate, for a variety of potentials ranging from 0.4 to 0.7 V, the inverse of current density (j^{-1}) as function of inverse of square root of rotational speed ($\omega^{-1/2}$). ORR activity of $\text{Fe}_3\text{C@N-CNT}$ sample is significantly higher than Pt/C (20 wt.%) electrocatalyst when measured in terms of half-wave potential.

In addition to metal carbides, metal sulfides (M_xS_y) are also an essential type of catalysts for the ORR because of their ability to function admirably at both room temperature and higher operating temperatures [62, 63]. The natural presence of metal species in MOFs, in conjunction with organic ligands, provides opportunity for physicochemical properties of MOF-derived M_xS_y @carbon system to be tailored to the user's specifications. This is made possible by the existence of MOFs. Hu et al. reported creation of unique $\text{Co-C@Co}_9\text{S}_8$ DSNCs through the use of a MOF-engaged method [64]. A reaction involving sulfide ions and the ZIF-67 that is liberated during the breakdown of thioacetamide (TAA) might result in the production of metal sulfides and compounds. This reaction can take place during the synthesis of metal sulfides and related compounds. By finely adjusting the reaction time, one is able to exert excellent control over the degree of sulfidation produced by the ZIF-67. As a consequence of this, it is possible to produce a variety of hollow nanostructures, some of which include CoS(a-CoS) amorphous nanocages and yolk-shelled structures ZIF-67@a-CoS . After that, the amorphous CoS can be transformed into crystalline Co_9S_8 by going through an additional thermal annealing step while being exposed to an inert atmosphere. It is hypothesized that the Co-C nanocages that are contained within the Co_9S_8 shells are what supply active sites for electro-catalytic ORR. In addition, the outer Co_9S_8 shells have the potential to effectively insulate active sites of Co-C from any potential aggregation that may occur. Because of this, the $\text{Co-C@Co}_9\text{S}_8$ DSNCs provide desirable ORR performance in terms of a great stability, low overpotential, high current density, and high methanol tolerance capability.

1.5 Lithium Oxygen Batteries

For redox operations using oxygen, the storage of discharged products (such as Li_2O_2), and mass transportation, MOF-derived materials that have well-distributed catalysts, large pore volume, and well-defined pores are helpful. Cage-type graphitic porous carbon- Co_3O_4 ($\text{GPC-Co}_3\text{O}_4$) polyhedron material derived from core-shell MOFs (ZIF-8@ZIF-67) delivered good cycle life and

low charge potentials as cathode material for LOBs. It shows that the graphitic carbon component of the material, were responsible for enhancing the conductivity, mesoporous structures, and cage-type structures. [41]. Besides this, graphene/graphene-tube nanocomposites, [65] Co_9S_8 @carbon porous nanocages, [66] $\text{ZnO}/\text{ZnFe}_2\text{O}_4/\text{C}$ nanocages, [67] $\text{g-Fe}_2\text{O}_3/\text{carbon}$, [68] and cobalt-manganese oxide, [69] reported for LOBs as cathode materials. Before LOBs can achieve the requirements for commercial applications (such as cycling durability, round-trip efficiency, and energy density), there are still several basic and technological difficulties that need to be addressed [70]. Because the carbon components of MOF-derived materials are susceptible to breakdown in presence of Li_2O_2 , these materials will have poor cycling stability [71]. Efforts to improve the carbon's stability by lowering functional groups on its surface and the number of flaws may serve as sources of inspiration for future endeavors in this area [71]. For the purpose of guiding the design and synthesis of MOFs to be used in LOBs, it will be extremely beneficial to have deeper understanding of LOBs' fundamental chemistry.

MOFs that contain accessible OMSs were shown to be capable of leading to considerable oxygen enrichment within framework by Li and co-workers [72]. The primary discharge capacity of Mn-MOF-74-Super P cathode under 1 atmosphere of O_2 at room temperature was $9,420 \text{ mAh g}^{-1}$, which was more than 4 times MOF-free cathode' discharge capacity [72]. Utilizing bimetallic MOF, such as MnCo-MOF-74, is one way to obtain an additional improvement [73]. The increased efficiency and reversibility were both attributed to synergistic integration of Mn-metal clusters and Co-metal clusters [73]. Electrochemical processes may be affected, to some degree, by size of particles as well as existence of defects. Particles of smaller size and with less perfect structure could be able to supply more active sites, which would increase amount of oxygen that was taken in and offer the prospect of a catalytic influence [74].

MOFs can be utilized as a membrane that is oxygen-permeable to protect lithium-air battery electrodes from carbon dioxide and moisture in the surrounding atmosphere. To construct MOFs with functional groups so that they behave in a favorable way with gas. It's possible that the use of MOFs for gas separation will provide us with some ideas and motivation. Mixed matrix membrane (MMM) was produced by integrating polydopamine-coated MOF (CAU-1-NH_2) into polymethylmethacrylate (PMMA) matrix. This was done in order to create the membrane [75].

Because of the presence of -NH_2 in CAU-1- NH_2 and -C=O in PMMA, as well as hydrophobic behavior of PMMA, the MMM was endowed with good hydrophobic behavior, oxygen permeability, and the ability of CO_2 capture. This enabled the lithium-air battery to maintain its cycling stability in ambient air with relative humidity of 30%.

The use of MOFs for LOBs as a cathode material is still completely unexplained despite widespread interest in the topic. Both the mechanism behind electrochemical process as well as function of MOFs in LOBs are not completely known at this time. In addition, there are a few essential problems that have still to be solved, the first of which is that the accumulation of electrolyte and product may obstruct active sites and pores of MOF. Second, during electrochemical process, there is the possibility that the active intermediates will degrade MOF structure. Finally, when material was used as a membrane, functional active sites might get gradually occupied until they reached saturation, which eventually resulted in a poorer adsorption performance and a corresponding decrease in the material's electrochemical performance.

1.6 Problem statement

- To develop a stable and active catalyst better than noble metals for OER.
- Enhancing stability and activity of ZIF-67.
- To enhance the durability of ZIF-67.

1.7 Research Objectives

To overcome the existing challenges in metal air batteries, following objectives were identified.

- To prepare and characterize catalyst for oxygen electrode in MABs.
- Improve durability and stability of ZIF-67 by addition of Mn and rGO.
- Synthesize a catalyst with low overpotential and Tafel slope values.
- To investigate electrochemical results of ZIF-67 and its composites.

1.8 Scope of Study

The following scope was established to ensure that the research would be carried out in the time available:

- Preparation of ZIF-67, 1-5 wt% rGO/ZIF-67 and 1-5 wt% rGO/Mn ZIF-67.

- The following characterization techniques were used FTIR, SEM, Raman and XRD.
- Electrochemical study of ZIF-67, 1-5wt% rGO/ZIF-67 and 1-5 wt% rGO/Mn ZIF-67. Cyclic voltammetry, Chronopotentiometry, EIS, and LSV.
- To compare experimental and predicted values of activity by application of MABs in study.

1.9 Chapter Summary

This thesis comprises of five chapters. The exposure of each chapter is given in following chapters.

- **Chapter 1** delivers vision of subject, background and applications of MOFs. It also clarifies problem statement, research objectives and scope of planned study.
- **Chapter 2** will sketch the literature review achieved to describe the previous work done on the MOF specifically.
- **Chapter 3** covers the methodology related to the sample preparation and characterization.
- **Chapter 4** delivers results and discussions. The material characterization, experimental, electrochemical results to compare the experimental and the predicted values and its consequences.
- **Chapter 5** reviews all the findings and conclusions in the current study and provides the future recommendation for the related work.

Chapter 2

Literature Review

2.1 Literature review

MOFs materials can give high catalytic performance in the field of electrocatalysis and can construct hollow structures with controllable size and tunable morphology through an acceptable combination of organic ligands and metal centers. This allows for the formation of MOFs materials. In general, the surface areas of MOF materials are large, and these materials also have their own unique nanopore architectures. When it comes to boosting OER and ORR reactions, both qualities might be seen as beneficial. In addition, the production of significant quantities of N-doping as a byproduct of the pyrolysis of MOFs as precursors makes ORR and OER processes more likely to occur. These reactions have the potential to modify carbon material's electronic structure and generate active centers of $M-N_x$, both of which contribute to increase in number of bifunctional catalytic active sites in an efficient manner.

Zeolite-imidazole framework, often known as ZIF, is one of the many different forms of MOFs that has been used widely in development of bifunctional catalyst. This is due to the versatility of the framework as well as the usage of transition metals as the framework center. It is projected that ZIF-67 will be a potential candidate for development of bifunctional catalysts. This is because transition metal cobalt has remarkable catalytic capability for OER and ORR. Calcination and carbonization at a temperature of 700 degrees Celsius were necessary to manufacture nano-cobalt particles that were encased in nitrogen-doped polyhedrons that were produced with carbon nanotubes (MOF-CNTs). This process took place in an atmosphere that contained hydrogen and argon. In order to get this process started, Wu et al. used ZIF-67 (precursor) [76]. MOF-CNTs displayed good electrocatalytic stability and activity in terms of OER and ORR. This may be owing to synergistic effect that is created when cobalt-rich nanoparticles are combined with CNTs and N-doped polyhedra. When measured against RuO_2 and Pt/C found in commercial products, the ORR and OER values of MOF-CNTs were shown to be superior. Both carbon nanotubes' structure, which is hollow, and carbon nanocages' structure, which is robust and porous, provided high-speed routes for the transport of electrolytes. The catalyst contained abundantly doped

nitrogen atoms as well as confined nanoparticles of cobalt, both of which induced additional active site and accelerated electron transfer for OER and ORR respectively. The MOF-CNTs possessed superior pore structure, an excellent specific area, and an excellent degree of graphitization, all of which were helpful to the process of improving stability and activity of bifunctional catalyst. This was achieved by graphitizing MOF-CNTs to a high degree.

It is essential to bear in mind that the activity of the catalyst as well as its stability will be directly impacted by the particle size as well as metal is spread throughout the substance that was generated from ZIF. ZIFs' transmission of active substances, surface area, and ratio of active site can all be increased by use of a particle size that is more suited to the environment and has a distribution that is more uniform. Recently, Li and colleagues have discovered a method that is effective in altering the size of Co nanoparticles that are included within ZIF materials. Graphitized carbonitride (g-C₃N₄) and glucose (Glu) were both injected at the same time for the first time using this technology, which made it the first adjustment strategy [77]. During the pyrolysis of imidazole and cobalt ions, the incorporation of g-C₃N₄ and Glu has been shown to effectively reduce the size of both cobalt particles and polyhedron. This procedure results in production of nitrogen-doped graphite electrocatalysts and bifunctionally active carbon-supported cobalt nanoparticles. This is accomplished through the synthesis of bifunctionally active carbon-supported Co nanoparticle. This is accomplished by limiting ZIF-67's growth rate. In addition, incorporation of C₃N₄ has potential to encourage the development of bamboo carbon nanotubes on surface of the polyhedron, which are then encapsulated by nano-cobalt particles. As a result of electrical interaction between metal nanoparticles and carbon nanotubes, it has been demonstrated that metal nanoparticles that have been enclosed in carbon nanotubes are able to increase effective catalyst activity. With this procedure, the ZIF-67 crystal size could be adjusted to range of 0.31-0.93 μm, while size of Co NP could be adjusted to range of 9.5-46.6 nm. Because of variables such as the smaller ZIF-67 polyhedra' even distribution, enhanced efficiency of active sites, and powerful Co-pyridyl-N coupling effect, catalyst displayed outstanding catalytic activity in both ORR and OER.

During the synthesis of ZIF-67, part of the cobalt in the precursor was replaced with zinc, which resulted in an improvement in the catalyst activity. Expulsion of zinc during high-temperature pyrolysis was found to be the cause of the observed improvement. This led to the creation of

catalysts with a porous structure and greatly enhanced specific surface area. This was accomplished by pyrolyzing the zinc at elevated temperature. Dispersion and size of cobalt nanoparticles were altered in the interim by adjusting ratio of zinc ions to cobalt ions in the precursor. This was done to prevent the cobalt particles from becoming clumped together during process of catalysis. The pyrolysis of a bimetallic Co/ZnZIF mixture resulted in the production of carbon nanomaterials (porous). These porous carbon nanomaterials that is porous and carbon nanotubes that was loaded with 14nm cobalt nanoparticles [78]. It was discovered that the catalytic efficacy was outstanding for both function of catalyst ($E_{j10}(\text{OER})-E_{1/2}(\text{ORR})=0.65\text{V}$) and exceptional long-term stability in both ORR and OER can be attributed to presence of numerous N-doped nanotubes, highly graphitized carbon, hierarchical mesoporous and microporous structures, as well as the uniform dispersion of nano-Co particles. In addition, this extraordinary long-term stability can also be due to presence of nano-Co particles. Wang et al. were able to generate a highly effective bifunctional electro-catalyst with a core-shell structure by first subjecting ZIF-8@ZIF-67 to hydrothermal treatment and then carbonizing the mixture [79]. They started by synthesizing ZIF-8 with just the zinc ion precursor in it. Because dimethylimidazole was present, it was simple to coordinate cobalt ions on surface of the crystals throughout the process of successfully fabricating core-shell structural ZIF-8@ZIF-67 crystals. The one-of-a-kind core-shell structure had the potential for interactions that were synergistic, while also integrating the benefits of both ZIF-67 and ZIF-8. This might result in increased catalytic activity for oxygen release and oxygen reduction.

It is possible to manufacture a variety of active centers inside the MOF material by including more than one metal in the synthesis process. These centers will have additive rather than additive effects. To boost OER catalytic activity, metallic nickel was typically included in the Co-MOF matrix in most cases. The bimetallic CoNi-MOF composite was used as precursor in Ning et al. preparation of porous Nitrogen-doped carbon coated CoNi alloy nanoparticle, which they referred to as CoNi@N-C [80]. Altering the proportions of cobalt and nickel present in the precursor, as well as the temperature at which the pyrolysis was carried out, led to the discovery of the optimal ratio for the $\text{Co}_1\text{Ni}_1@\text{NC}$ material. At the same time, the material displayed a distinct porosity along with a homogeneous distribution of CoNi alloy nanoparticles, significant quantity of

nitrogen atoms doping, and distributed active sites of CoNi-N_x. These characteristics suggested that the material might give remarkable catalytic activity in the OER and ORR processes. After pyrolysis, carbon polyhedron fell apart due to the weak binding force that existed between the organic ligands and the nickel, which served as a reminder to us that a more appropriate inclusion approach needs to be designed. Following the carbonization of MOF materials, a successful process for decorating additional metals has been established using adsorption or different methods. This is in addition to the strategy of directly introducing more metal ions into the precursor, which has proven to be effective. By modifying both pyrolysis temperature and quantity of Fe doped atoms, Pendashteh et al. were able to successfully produce a highly efficient electrocatalyst for ORR and OER. Co-ZIF-9 served the purpose of a sacrificial precursor. This resulted in the electrocatalyst having both ORR and OER functionality [81]. Theoretical and experimental evidence demonstrated that adding Fe to a catalyst considerably enhanced its activity for OER and ORR by raising the total number of electrons transported.

It is possible to improve catalytic performance of bifunctional catalyst by employing a method that is both efficient and effective, and this opens up the possibility of doing so. This method involves post-processing of materials that have been created from MOFs. By sulfiding, phosphating, selenizing, or oxidizing MOF materials, the authors of certain studies were able to produce good bifunctional catalytic activity. Co-sintering the catalyst with precursors like sulfur powder, selenium powder or sodium dihydrogen phosphate in the same heating chamber at temperatures ranging from 200 to 450 degrees Celsius is the most typical method. These approaches, unfortunately, have the potential to disrupt morphology of material and induce structural collapse. This will influence catalyst's surface area as well as transportation process, which will ultimately result in the MOF losing its activity. To establish stable activity in MOF materials, it is necessary to address two important factors: (1) taking use of synergistic impact that exists between active sites in MOF for ORR and OER, and (2) managing the subsequent treatment in such a way as to retain the integrity of the active sites that were present initially. These two aspects are equally important to consider when trying to achieve a steady bifunctional activity in MOF materials. By accurately adjusting the level of Co-CN oxidation, Ding et al. were able to successfully manufacture a variety of Co-Co₃O₄-based nanostructures that were embedded in hollow N-doped

carbon polyhedrons (HNCP). These nanostructures were embedded in carbon polyhedrons [82]. They discovered that the length of calcination in an environment including O₂ and Ar had a discernible impact on morphology of both HNCP and Co-Co₃O₄. Co particles underwent a progressive transformation into Co/Co₃O₄ with core-shell structure during first step of calcination process. During the oxidation process, most of Co/Co₃O₄-NP core shell transformed into Co@Co₃O₄-NP yolk shell, and few Co₃O₄-NP hollow were produced. Bulk of Co@Co₃O₄-NPs yolk shell in the Co₃O₄/HNCP-40 combination transformed into Co₃O₄ NPs hollow when the level of oxidation was increased even more, while part of structure of yolk shell remained intact. When the oxidation process was finished, structure of egg yolk and shell was eventually transformed into hollow Co₃O₄ NPs. Fortunately, the level of oxidation could be well controlled, which resulted in the hollow carbon-based framework being kept in excellent condition.

In the meantime, Co₃O₄/HNCP-40 yolk-shell displayed greatest OER and ORR activity. It was due to multiple oxygen vacancies, additive effect of CoO and Co²⁺; the efficient mass transfer facilitated by the yolk shell and hollow N-doped carbon. This led to that ORR and OER dual-function activity was best demonstrated by the yolk-shell combination of HNCP-40 and Co₃O₄. Annealing treatment that is conducted on MOFs, the post-processing of MOFs consists of loading various catalytic particles onto MOF-derived materials. This is done in an effort to further increase the catalytic performance of the MOFs. To create porous Co₃O₄@Z67-N700 while maintaining outstanding activity, Li and his colleagues regulated oxidation level of ZIF-67. They did this by using hydrothermal approach to evenly coat carbon shell surface with the CeO₂ nanoparticles [83]. It was determined that the synergy between Co₃O₄ and CeO₂ was responsible for the catalyst's remarkable electrocatalytic bifunctional activity ($E_{j_{10}(\text{OER})} - E_{1/2(\text{ORR})} = 0.70\text{V}$), measured at electrode. Vacancies of oxygen on Co₃O₄ and CeO₂ boosted adsorption of oxygen on interface, accelerated activation of oxygen that was adsorbed to become oxygen O²⁻ and reduced lack of oxygen that was present during the ORR, which resulted in an improvement in the activity of the ORR. The contact between Co₃O₄ (CoOOH/Co³⁺) and CeO₂ (Ce⁴⁺/Ce³⁺ and oxygen vacancies) provided the OER with access to additional electrochemically active sites, which considerably the smooth/generation transmission of active species (O₂⁽²⁻⁾/O⁻) and high charge transfer. Additionally, this interaction produced more active sites for OER.

MOF-derived materials are currently intensively explored in field of electrocatalysis' advanced materials. This is primarily attributable to the controllability, modifiability, and versatility of MOF-derived-materials. This considerable investigation of materials generated from MOFs can in part be attributed to the remarkable traits and qualities of these materials. In realm of MOF-derived-materials, the focus of study has mostly been on investigating the materials' catalytic activity for ORR. Comparatively little attention has been paid to determining the materials' electrocatalytic performance for OER. This dichotomy exists because the electrocatalytic performance of these materials for OER has not yet been deemed adequate. Directly integrating MOF materials that have strong ORR catalytic activity with extra components like Ni nanoparticles for increased OER catalysis. However, this strategy only produces a slight improvement and has a negative effect on activity of ORR. The OER activity can be greatly increased with application of intensive oxidation or alternate calcination treatments; however, these treatments also result in a large reduction in the ORR activity. This can happen even though the treatments can lead to excellent OER activity. To properly synthesize bifunctional oxygen catalysts, there are still a few areas that need additional research as well as improvements. These areas are as follows:

- i) It is necessary to integrate the catalytic capabilities of OER and ORR while taking into consideration the synergistic effect that can occur between the active sites of both reactions in order to build bifunctional oxygen catalysts with any degree of success. This necessitates the development of novel synthesis procedures that can meet the bifunctional criterion in MOF-derived materials without relying on the external supplementation of the second catalytic function. Taking into full consideration synergistic effect between OER and ORR active sites.
- ii) Precisely regulating degree to which subsequent treatment is performed while simultaneously improving the electronic structure and morphology to achieve a balance between the catalytic activity required for ORR and OER.
- iii) Developing innovative synthesis methods that make most of the benefits of MOF materials and strike a healthy balance between catalytic activity and the inherent

stability of the material. This is very necessary in order to derive the most possible benefit from the use of MOF materials.

Table 1: ZIF-67 reported catalytic performance values in literature.

<i>Catalyst</i>	<i>Substrate</i>	<i>Electrolyte</i>	<i>Scan Rate</i> (mVs^{-1})	<i>Tafel</i> ($mVdec^{-1}$)	<i>Overpotential</i> (mV)	<i>Ref.</i>
<i>ZIF-67</i>	GCE	1 M KOH	5	235	400	[84]
<i>ZIF-67</i>	RDE	1 M KOH	5	96	400	[85]
<i>ZIF-67</i>	GCE	1 M KOH	5	82	352	[86]
<i>ZIF-67</i>	GCE	1 M KOH	5	128.2	408	[87]
<i>ZIF-67</i>	NF	1 M KOH	5	98	400	[88]
<i>ZIF-67</i>	GCE	1 M KOH	5	74	546	[89]
<i>ZIF-67</i>	RDE	1 M KOH	5	105	334	[90]
<i>ZIF-67</i>	GCE	1 M KOH	1	-	420	[91]
<i>ZIF-67</i>	GCE	1 M KOH	5	88.3	390	[92]
<i>ZIF-67</i>	GCE	1 M KOH	2	83.8	410	[93]
<i>ZIF-67</i>	GCE	1 M KOH	2	147	530	[94]
<i>ZIF-67</i>	GCE	0.1 M KOH	5	125.5	530	[95]
<i>ZIF-67</i>	GCE	0.1 M KOH	5	122	480	[96]

Through the introduction of intrinsic defects and the use of a fair quantity of heteroatom doping, metal-free carbon materials are able to give good dual-function electrocatalytic activity. Nevertheless, their catalytic performance, particularly their stability, has room for additional development. The serious corrosion of carbon at high voltage that occurs during the OER catalytic process will have a significant and negative impact on life cycle of ZABs. In order to optimize performance of dual function catalysts and boost their stability, it is essential to incorporate a proper proportion of metal into materials based on carbon. Because of the numerous opportunities that lie ahead for them in the field of catalysis, single-atom catalysts, MOFs-derived materials, and graphene-supported materials have garnered great deal of attention [97-99].

Ever since graphene was discovered, its one-of-a-kind structure and performance have been the subject of extensive research. 2010 marked the year that the prestigious Nobel Prize in Physics was bestowed upon the researcher who was responsible for the discovery of graphene. Graphene has some remarkable properties, such as high carrier mobility of up to $10000 \text{ cm}^2 \text{ V}^{-1} \text{ s}^{-1}$, thermal conductivity ranging from 3000 to $5000 \text{ W m}^{-1} \text{ K}^{-1}$ at ambient temperature, significant surface area of approximately $2630 \text{ m}^2 \text{ g}^{-1}$, an exceptional optical transparency of around 97.3%, and an impressive mechanical strength with a Young's modulus of 1.0 TPa. Because of its remarkable material properties, graphene can perform both the role of a carrier for dual-function catalysts and the role of a catalyst on its own. These properties include great thermal and electrical conductivity as well as high specific surface area.

A high-efficiency method for synthesis of composite catalyst has been contemplated, and it involves loading transition metal nanoparticles onto materials made of graphene. Because of the sequence in which transition metals are ranked in terms of their electrocatalytic activity, it might be difficult to fulfill the requirements for both the ORR and the OER. ORR activity order in electrocatalytic reactions goes as follows: $\text{Ni} > \text{Mn} > \text{Cu} > \text{Co} > \text{Fe}$, whereas the OER activity order goes as follows: $\text{Co} > \text{Cr} > \text{Zn} > \text{W} > \text{Ni} > \text{Fe/Cu/Mn} > \text{Mo}$. As a consequence of this, it is difficult for single metal to satisfy prerequisites of both ORR and OER at same time. To solve this problem, it is absolutely necessary to use an alloy that is a blend of several different metals. This strategy is essential in order to solve the issue at hand in an efficient manner [100, 101]. It is possible to do what has to be done by combining a heat reduction system with a 2-step sol-gel process, Khani et al. were able to synthesize a series of single metal nanoparticles consisting of iron, nickel, and cobalt as well as their ternary and binary alloys. These nanoparticles were encased in a graphite carbon shell [102]. Several different ex-situ characterizations suggested that the most outermost layer of graphite had been electrochemically peeled away as a result of the extreme circumstances that were present during the electrochemical process. The electrically modified graphene inner layer did not flake and stayed unbroken, which effectively prevented the bulk of metal particles from taking part in the electrocatalysis process. This leads one to believe that some metal nanoparticles were not entirely encased by graphite shell, which resulted in the formation of an extra active site for electrocatalytic activity, particularly in the process of OER. As

electrochemical reaction progressed, there was a corresponding increase in the concentration of metals near the surface of the sample that had higher oxidation state. This finding suggests that a fraction of the metal nanoparticles was not sufficiently encapsulated within graphite shell. This was demonstrated by the fact that the quantity of metal close to the surface that was in a highly oxidized state increased. Because of this, the performance of the Ni-Fe binary system was encouraging in terms of OER, whilst the performance of the Co-Fe binary system was the most successful in terms of ORR. Ternary alloys NiCoFe that are encased in graphite carbon shell ($\text{G-Ni}_{1/3}\text{Co}_{1/3}\text{Fe}_{1/3}$), which are manufactured by changing compound's metal ratio, have potential to both achieve an effective electrocatalysis which leads to practical MABs. This is because the compound is manufactured by changing compound metal ratio. In addition to the utilization of metal nanoparticles, loading graphene with transition metal hydroxides, sulfides, oxides, and nitrides is an additional effective technique for synthesis of bifunctional catalysts. In contrast to metal particles, metal compounds that have a greater valence have a lower probability of becoming oxidized, which results in a longer lifespan for the catalytic reaction that they catalyze. By exposing cobalt-containing precursors and graphene to pyrolysis in ammonia atmosphere at a temperature of 500 degrees Celsius, Zou et al. were able to successfully create interconnected amorphous cobalt nitride (CoN_x) nanoparticles within a three-dimensional (3D) N-doped graphene aerogel (NGA) [103]. Excellent catalytic performance was obtained by the CoN_x -NGA for both ORR and OER ($E_{j10}(\text{OER})-E_{1/2}(\text{ORR})=0.6\text{V}$). This was made possible by the dual-active CoN_x and the hierarchically porous structure of the graphene aerogel. In addition to this, a different metal can be added to metal nitride, and atomic ratio of the two metals can be changed to improve electrocatalytic performance of catalyst. Researchers team headed by a scientist He Pyrolyzing matching graphene and metal hydroxide allowed him to make uniform and ultrafine $\text{Ni}_x\text{Co}_y\text{N}$ nanoparticles that were anchored to N-doped reduced graphene ($\text{Ni}_x\text{Co}_y\text{N}/\text{NrGO}$) [104]. An effective dual-function catalytic material was created when metal nitride uniformly dispersed was mixed with highly porous conductive NrGO. By modifying metal atomic ratio, it was discovered that $\text{Ni}_{2.25}\text{Co}_{0.75}\text{N}/\text{NrGO}$ hybrid displayed higher durability and kinetic activity for both OER and ORR. This was the case even though the hybrid had lower atomic ratios of the two metals. In addition, $\text{Ni}_{2.25}\text{Co}_{0.75}/\text{NrGO}$ electrocatalyst-assembled ZABs had a high value 193 mW cm^{-2} (power density) and 864 W h kg^{-1} (weight energy density). These batteries also exhibited a cycling

capability up to 166 hours at current density of 10 mA cm^{-2} and charge/discharge voltage gap of 0.72 V.

In addition, incorporation of two distinct kinds of metals and compounds of metals enables each component to contribute to the activity of either ORR or OER. Furthermore, successfully combining the benefits that each offers as a means of building dual-function catalysts is yet another way to do this. On the other hand, simple mixing will lessen their intrinsic activity and might possibly have a negative effect on the ORR/OER performance. The synergistic impact that might occur between several metal phases can significantly boost the activity of OER and ORR. Using sol-gel polymerization, Fu and his colleagues were able to develop Ni-MnO/rGO materials. These materials featured thin nanoparticles of Ni-MnO that were uniformly dispersed on a porous three-dimensional graphene network. MnO was determined to play the most important part in the ORR activity, whilst Ni was responsible for OER activity. Both of these components contributed to the overall activity [105]. Remarkably, catalytic performance of Ni-MnO/rGO in a 0.1M solution of KOH topped that of any individual metal. The ORR half-wave potential ($E_{1/2}$) of Ni-MnO/rGO was measured at 0.78V, while the OER overpotential (E_{j10}) was measured at 1.6V. Zinc-air batteries (ZABs) that are based on Ni-MnO/rGO display a remarkable combination of high voltage efficiency and robust charge-discharge cycling for more than 100 cycles. This is a significant achievement. The outstanding bifunctional performance is the consequence of a synergistic effect that was produced by the integration of MnO and Ni metals, in addition to high conductivity and expansive surface area of 3D porous rGO aerogel. This resulted in exceptional bifunctional performance.

Extended electrochemical cycling increases the chance of agglomeration of metals and their compounds, which is a fundamental worry that impacts durability and catalytic activity of catalysts. This is a problem because agglomeration of metals and their compounds reduces the catalytic activity of catalysts. This phenomenon emerges as a consequence of long-term cycling, which results in an increase in the possibility that agglomeration will take place. In order to extend cycle life of rechargeable ZABs and stop metal particles from clumping together, it is very necessary to use an anchoring method that is successful. The collection of metal particles is significantly hampered by employing this approach, which plays vital role in process. Afshin et al.

developed novel sort of non-noble metal catalyst, which they referred to as NiCoMnS₄/N-rGO. This was accomplished by attaching N-rGO with nanoparticles of metal sulfide using straightforward anion exchange method [106]. Because of this one-of-a-kind anchoring and synergistic action, the catalyst possesses superior electrocatalytic activity as well as acceptable durability (OER $E_{j_{10}} = 1.64\text{V}$ and ORR $E_{1/2} = 0.81\text{V}$). In addition to this, the NiCoMnS₄/N-rGO-based air cathode that was used to assemble the rechargeable ZAB displayed high energy density, rate capability, outstanding cycle stability and capacity. The unavoidable phase transition of some metastable phases, such as sulfides, in acid or high-alkaline electrolytes has negative impact on the electrocatalytic performance of the system. This phase change is an inevitable and intrinsic occurrence that cannot be avoided in any way [107, 108]. It is possible that one of the most essential ways to increase the stability of dual-functional catalysts is to develop efficient protection techniques with the goal of preventing or minimizing the inevitability of phase shift. In order to encapsulate Co₉S₈ nanoparticles within the graphite layer of a three-dimensional graphene material, Li et al. utilized a method that is known as the soft template auxiliary approach. This method is both straightforward and highly effective. The end product, which was given the name Co₉S₈@3DrGO, had a very porous structure and a substantial amount of surface area [109]. Because of its one-of-a-kind core-shell structure, which guarantees an excellent distribution and size of Co₉S₈, electrocatalytic ORR and OER performance of Co₉S₈@3DrGO was extraordinarily effective. Most notably, it maintained an extremely high level of catalytic durability even when exposed to very alkaline solutions. This study highlights potential of effective protective measures for the design of very stable bifunctional catalysts based on cobalt sulfide. When used to ZABs, this cobalt sulfide-based catalyst has high 83.5 mW cm⁻² (power density) and outstanding activity. In addition, one method that can be taken into consideration is the optimization of metastable phase interface of crystal phase to increase stability of the system by developing lattice structure that is more rational. However, additional research is required in the area of the design of electrocatalysts that can perform two functions simultaneously.

In point of fact, the method of integrating graphene materials by transition metals as a dual-function catalyst for oxygen can also be applied to variety of other carbon-based materials such as carbon nanotubes, carbon nanosheets, and C₃N₄, amongst others. This is because graphene is two-

dimensional material. This is because graphene is two-dimensional material. Both ORR and OER can benefit from enhanced catalytic performance if the catalyst is doped with the appropriate heteroatoms and its specific surface area is modified. In a nutshell, graphene has been the subject of a significant amount of research as an innovative material over the past several years. Additionally, its application in the field of electrocatalysis has undergone significant development and improvement, whether it is used as catalytic species itself or as carrier. The fulfillment of diverse catalytic needs can be accomplished through incorporation of wide variety of metal and compounds. Maximizing the catalytic effect can be accomplished by the efficient combination of the benefits offered by a wide variety of components. The most significant drawback of graphene-supported catalysts, on the other hand, is that their bifunctional catalytic stability and activity are not yet on par with those of other cutting-edge materials. Consideration should also be given to the following areas to concentrate on to make improvements:

- i) It is vital to develop innovative anchoring strategies that successfully hold the catalytic particles onto or within the graphene material to prevent the loss of activity and agglomeration of nanoparticles that occurs during the process of electrocatalysis. This will allow for the prevention of the aggregation of nanoparticles. It is necessary to do this in order to keep the action going and stop the particles from clumping together.
- ii) It is essential to develop efficient techniques of synthesis that can optimize the size of catalytic particles and promote a uniform dispersion throughout the material in order to make complete use of graphene materials. This will allow graphene to be utilized to its maximum potential. Graphene can be employed more effectively, leading to improved performance and increased usage of its capabilities, if an even dispersion of the material can be achieved.
- iii) To achieve the goal of enhancing interaction between catalytic particles and the graphene substrate, a comprehensive inquiry is being carried out with the intention of conducting an in-depth analysis of combined catalytic effect of a number of distinct components. The purpose of this investigation is to gain a better knowledge of how the various components work together to contribute synergistically to the catalytic activity,

which ultimately leads to an interface that is optimal between the particles and the graphene substrate.

Chapter 3

Materials and Methods

3.1 Raw material

All reagents and chemicals used in the preparation of ZIF 67 and their rGO-based composites, i.e., 1-5wt% rGO/Mn ZIF-67, 1-5wt% rGO/ZIF-67, were analytical grade (Sigma-Aldrich products), used without further purification. The products constitutes of 2-methylimidazole, cobalt nitrate hexahydrate ($\text{Co}(\text{NO}_3)_2 \cdot 6\text{H}_2\text{O}$), manganese nitrate hexahydrate ($\text{Mn}(\text{NO}_3)_2 \cdot 6\text{H}_2\text{O}$), concentrated sulfuric acid (H_2SO_4), sodium nitrate (NaNO_3), sodium hydroxide (NaOH), methanol, graphite powder, potassium permanganate (KMnO_4), hydrazine hydrate ($\text{NH}_2\text{NH}_2 \cdot \text{H}_2\text{O}$), hydrogen peroxide (H_2O_2), DI water, Nafion.

3.2 Synthesis of ZIF-67

ZIF 67 was synthesized by dissolving 3.15 g of 2-methylimidazole in 50 mL of methanol; after the addition of 1.45 g of $\text{Co}(\text{NO}_3)_2 \cdot 6\text{H}_2\text{O}$ to this solution, a purple color appears. The mixture was stirred overnight at room temperature. Solid product was obtained by centrifugation of reaction mixture at 4500 rpm. The product was refined by washing with methanol and centrifuging it for 10 minutes at 4500 rpm. This step was performed three times to ensure that all contaminants were removed [110]. The product was then dried overnight at 60 °C in vacuum oven.

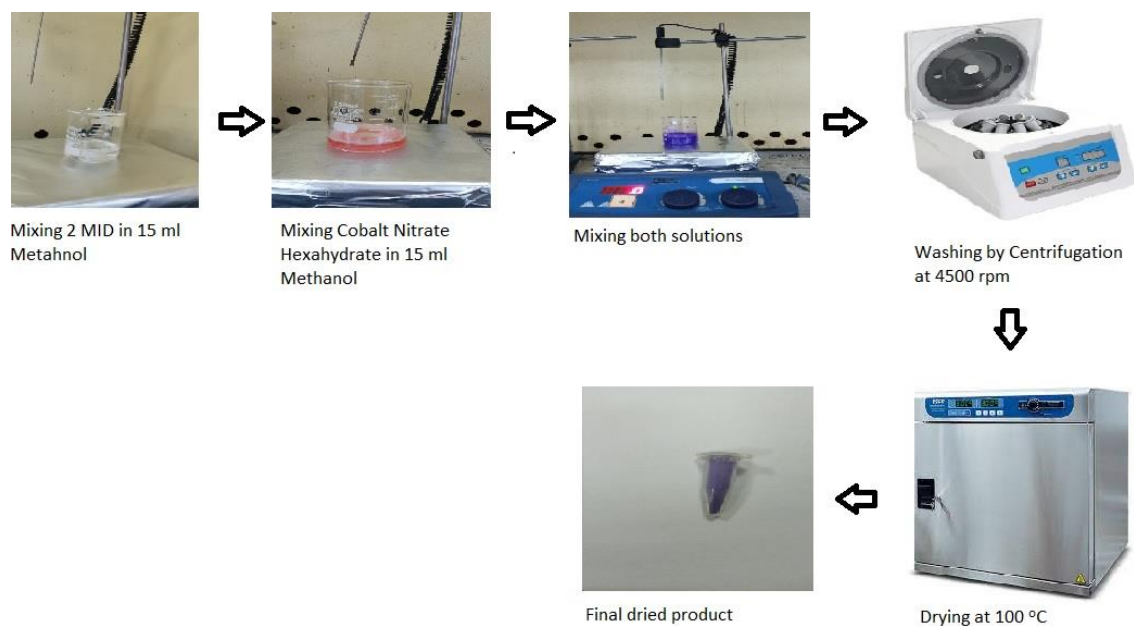


Figure 2: Schematic diagram for synthesis of ZIF-67

3.3 Synthesis of rGO/ZIF-67

It was determined that the solvothermal method was the most effective way to prepare the 1-5 wt% rGO/ZIF-67. In beginning, calculated amount of 1–5 wt% GO is introduced one at a time in 10 ml of DI water, which is then ultrasonically agitated for 1 hour. In order to prepare the ligand solution, 1.232 grams of 2-methylimidazole were dissolved in 15 milliliters of methanol. In order to prepare the metal solution, 1.092 grams of $\text{Co}(\text{NO}_3)_2 \cdot 6\text{H}_2\text{O}$ were dissolved in 15 milliliters of methanol. While continuously stirring, a step-by-step addition of the linker solution was made to the metal solution in the pursuit of a uniform consistency. Following homogenous solution was placed inside autoclave, and then it was tightly sealed before being heated to a temperature of 120 degrees for 19 hours. The product was centrifuged for ten minutes at a speed of 4,500 revolutions per minute. After the product had been acquired, it was dried in an oven at 100 degrees Celsius for a full 24 hours and then washed three times with methanol [46].

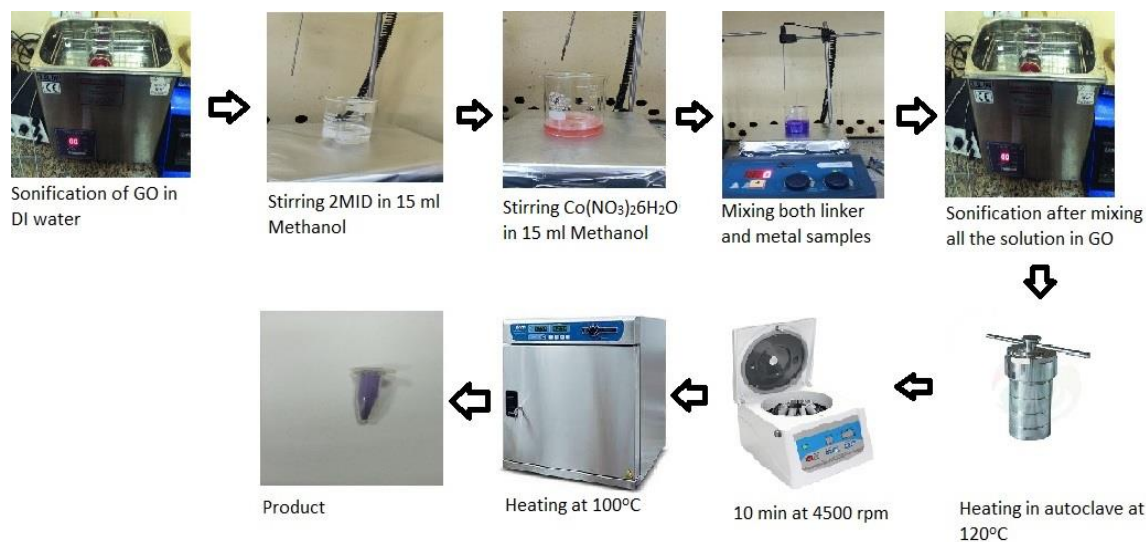


Figure 3: Schematic diagram of 1-5wt% rGO/ZIF-67

3.4 Synthesis of rGO/Mn ZIF-67

In addition, solvothermal procedures were utilized to produce reduced graphene oxide-based Mn ZIF-67 composites. In the beginning, the calculated amount of 1–5 wt% GO is introduced one at a time in 10 ml of DI water, which is then ultrasonically agitated for 1 hour. To prepare the metal solution, 1.116 g $\text{Mn}(\text{NO}_3)_2 \cdot 6\text{H}_2\text{O}$ and 1.092 g $\text{Co}(\text{NO}_3)_2 \cdot 6\text{H}_2\text{O}$ were dissolved in 15 ml, then the homogeneous metal solution was added to the already prepared GO solution and sonicated for another 2 h. Whereas the ligand solution was also made by mixing 1.232 g of 2-Methylimidazole in 15 ml of methanol, the prepared linker solution was progressively added to the metal solution while stirring. The resultant homogenous solution was placed inside of an autoclave, sealed off completely, and heated to a temperature of 120 degrees for 19 hours. The product was centrifuged for ten minutes at a speed of 4,500 revolutions per minute. After obtaining the product, it was washed three times with methanol before being dried in an oven at 100 degrees Celsius for an

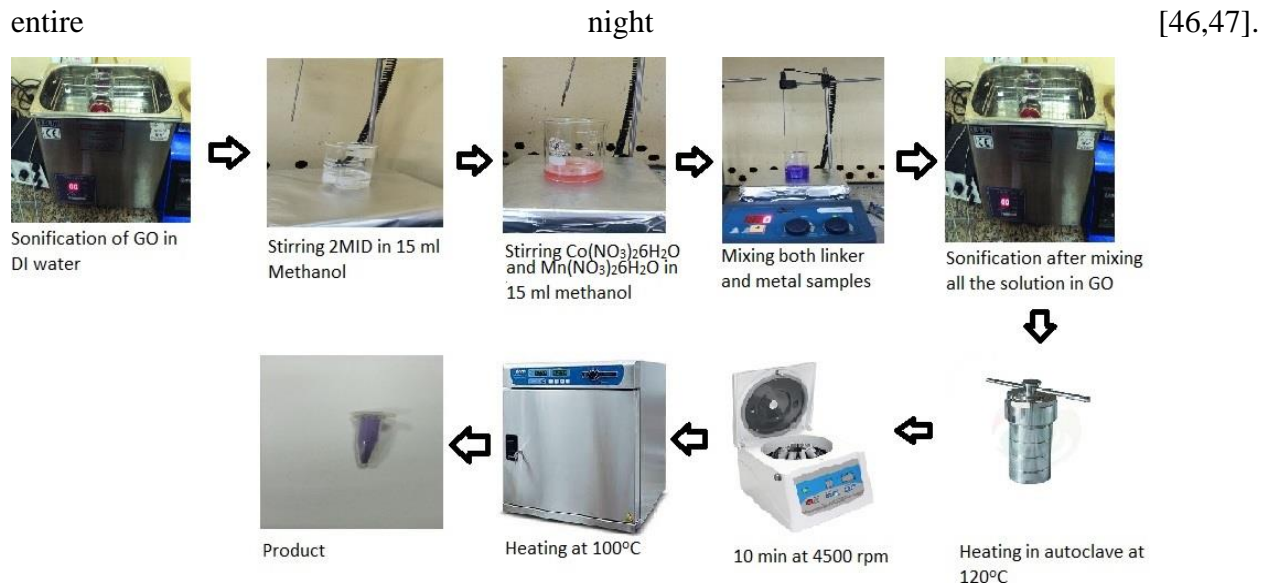


Figure 4: Schematic diagram of 1-5wt% rGO/Mn ZIF-67

3.5 Scanning Electron Microscope

The TEM and SEM are the two primary categories of electron microscopy. SEM microscopes all produce an electron beam that is extremely focused, which then strikes the specimen while it is contained in a vacuum chamber. Like reflection light microscopes, scanning electron microscopes are generally used to investigate surfaces of various materials. In SEM, electron beam is focused to point, and it is scanned across material in a consecutive fashion. Signals are emitted from specimen in each site, and those signals are captured by detectors. The signal from detector is synchronized with the known location of the beam on the specimen, and intensity of the signal is utilized to modulate picture pixel that corresponds to it. The signals that are captured in series are merged to create an image, the dimensions of which and the distribution of whose pixels are determined by the scan pattern that is selected. Typical electron energies are 1e30 keV [111].

3.6 X-Ray Diffraction

XRD methods are based on fact that crystals have the ability to diffract X-rays in recognizable pattern, which enables an in-depth investigation of the structural makeup of crystalline phases. Diffraction patterns that have been recorded contain the additive contributions of a number of different microstructural and macrostructural aspects of a sample. Investigations into the macro stresses, space group, chemical composition, lattice parameters, and qualitative phase analysis are

all possible when utilizing the peak position. It is possible to extract information on the crystal structure (occupancy, temperature factor or atomic positions), as well as information about the texture and quantitative phase analyses, based on the peak intensity. Last but not least, the shape of the peak provides information on the contributions to sample broadening (crystallite size and microstrains) [112].

3.7 Fourier Transform Infrared

FTIR spectroscopy, often known as "Fourier transform infrared" (or "FTIR") spectroscopy, is a versatile method for characterizing materials that are members of carbon family. This method, which is based on the way that IR radiation interacts with matter, can be utilized for the purpose of identifying and characterizing the constituents of chemical structures. The most important aspects of this technology are that it is non-destructive, that it can measure in real time, and that it is reasonably simple to implement. FTIR spectrum is a graphical representation of the transmittance, in terms of percent (T%) or absorption, in terms of units (A), versus IR frequency, expressed in terms of wavenumber (cm^{-1}). The absorption bands of an IR spectrum are distinguished from one another by the wavenumber at which the absorption occurs (which corresponds to the chemical bonds), as well as intensity of the absorption (which is proportional to amount of substance in the sample) [113].

3.8 Raman Spectroscopy

The Raman spectroscopy is a very powerful instrument for analysis of materials, which allows for the investigation of the properties of a wide variety of distinct materials. Since its discovery, Raman spectroscopy has been put to use to explore numerous properties of materials, including carbonaceous and inorganic properties. These investigations have resulted in the gathering of valuable information regarding the phases, functions, and flaws of the materials. In addition, the range of application of Raman analysis has been expanded to include biological and analytical disciplines as a result of the development of techniques such as surface and tip enhanced Raman spectroscopy. The reliability and adaptability of Raman instruments make them a potentially useful tool for doing on-site examination of a wide variety of materials [114].

3.9 Potentiostat

3.9.1 Overpotential

The most accurate method for determining OER and ORR activity of catalysts is the use of overpotential [115]. It is the difference between potential at given current density and 1.23 volts, which is reaction energy barrier. This gap is referred to as the potential barrier. In general, while determining ORR, we make use of onset potential and the half-wave potential ($E_{1/2}$), but when determining OER, we make use of potential and onset potential at 10 mA cm^{-2} ($E_{j_{10}}$). To have more direct activity evaluation in bifunctional catalyst, $E = E_{j_{10}} - E_{1/2}$ is used. This method is favored because it gives a clearer picture of the normal overpotential that is seen in ORR and OER reactions, and it has a direct connection to open circuit potential of MABs. In addition, the equation $E = E_{j_{10}} - E_{1/2}$ is utilized so that more direct evaluation of the activity that bifunctional catalyst is capable of can be performed [116].

3.9.2 Tafel Slope

The empirical formula known as the Tafel formula was first proposed by Tafel in the year 1905. Tafel formula is: $\eta = b \cdot (\log j / j_0)$.

Where b represents the gradient of the Tafel line, η represents overpotential, j_0 represents exchange current density and j represents current density.

Tafel slope is useful tool for analyzing kinetic process as well as the mechanism underlying electrocatalysis. When it is lower, the driving power necessary for reaction process, which applies to both ORR and OER, is reduced. This is the case regardless of how low it is. When going through ORR and OER, a good bifunctional catalyst should have relatively modest Tafel gradient.

The thermodynamic idea of exchange current density, denoted by j_0 , provides insight into the fundamental characteristics of reaction on electrode. The overpotential is based not only on the temperature but also on the composition of the electrodes and the concentration of reactive compounds that are present within the system. Temperature is the most important factor. Value, which is determined using Tafel curve, provides a direct reflection of the complexity of an electrode response and may be estimated using the curve. The exchange current density is a determining element in the internal component that determines the degree of polarization of

electrode. If current density is high, then the driving force, which is measured in terms of the external current density, must be relatively low for one electrode reaction to take place. When current density is low, driving force necessary for one reaction at electrode must be high. [116].

3.9.3 Stability

The cycle life of the MABs is closely related to stability of catalyst, which is another extremely significant scientific signal [117, 118]. By using chronoamperometry, CV, and several other tests in the 3-electrode assembly, we are able to directly identify the stability of catalyst, regardless of whether it is ORR or OER. Morphology and composition of the catalyst, which may be established by physical characterization techniques such as XPS, XRD, TEM, and SEM are used to evaluate catalyst's stability. This is perhaps the most essential point. Range of novel characterization technologies like in-situ XPS, XRD, TEM, and SEM have provided chances to better understand compositional and structural changes which happens while catalyst reacts. These opportunities have allowed for a better understanding of compositional and structural changes that happen [116].

3.9.4 Electrode Characteristics

Because fabrication of the working electrode is the goal of creating catalyst, certain physical and chemical properties, such as binding force, electrical conductivity, solubility, and wettability, are of utmost significance [119, 120]. To begin, the catalyst should have a high wettability, since this will shorten the amount of time that it takes for reactants to become separated from active sites within the catalyst. Second, it is important that the catalyst be securely connected to the substrate, particularly when the OER process is being carried out because a significant amount of oxygen will be produced. It is possible for the catalyst to become detached from the substrate if the link between them is not strong enough. When this happens, the electrode will become inactive. However, as an excessive amount of the binder would immediately impact wettability of material, also it increases resistance, it is not advisable to use an excessive amount of the binder. In recent times, a number of studies have concentrated their attention on in-situ development of catalyst directly on nickel foam or carbon paper [121]. The 3-D structure of this approach not only makes it simpler to contact electrolyte but also encourages the reaction products diffusion, but it also makes substrate and catalyst more stable, which is one of the benefits of using it.

Chapter 4

Results and discussion

4.1 Results and discussion

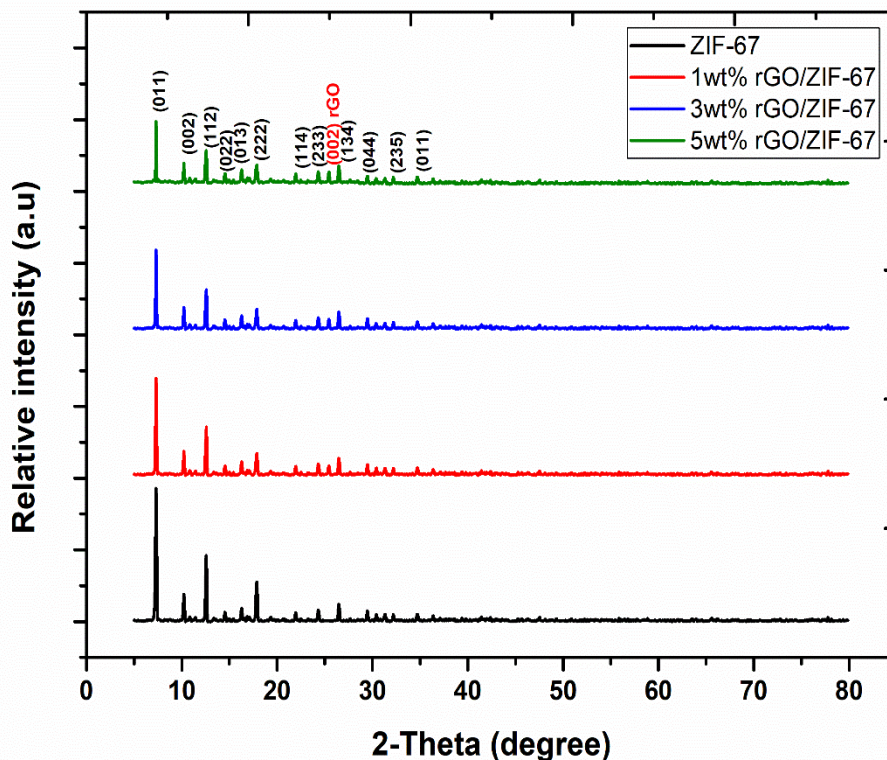


Figure 5: XRD of ZIF-67, 1wt% rGO/ZIF-67, 3wt% rGO/ZIF-67, 5wt% rGO/ZIF-67

Crystal phase and structure information of the samples were studied by XRD analysis of a ZIF-67 (reference) and 1-5wt% rGO/ZIF-67, 1-5wt% rGO/Mn ZIF-67 (Composites). Samples 1-5wt% rGO/ZIF-67, 1-5wt% rGO/Mn ZIF-67 and ZIF-67 showed the characteristic diffraction peaks of MOF. This observation provides evidence that ZIF-67 was successfully included into the composite that was produced. The prominent peaks that may be seen in XRD pattern of 1-5wt% rGO/ZIF-67 can be listed as: 7.35° (011), 10.5° (002), 12.65° (112), 14.68° (022), 16.35° (013), 17.9° (222), 22.95° (114), 24.45° (233), 25.59° (002), 26.49° (134), 29.54° (044), 32.47° (235) [122-124]. In specifically, the presence of rGO can be determined by the existence of a 2 peak

with a low intensity located at 25.59° (002) (CCDC no. #671073) [125]. It is also important to highlight that due to the mono- to few-layered structure of rGO, it is highly improbable that it will reflect a significant number of diffraction peaks [126]. In spite of this, the XRD examination has yielded fruitful data regarding the successful creation of the intended nanocomposite consisting of rGO and ZIF-67.

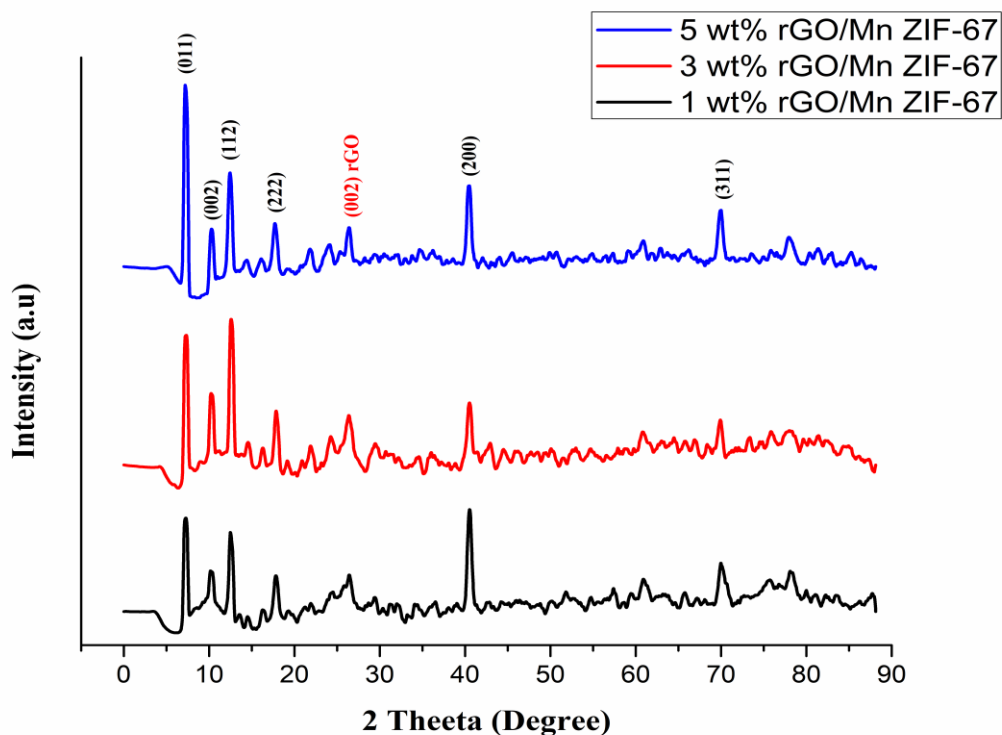


Figure 6: XRD of 1wt% rGO/Mn ZIF-67, 3wt% rGO/Mn ZIF-67, 5wt% rGO/Mn ZIF-67

The XRD pattern shows that there are peaks in 1-5wt% rGO/Mn ZIF-67 are: 7.35° (011), 10.5° (002), 12.65° (112), 17.9° (222), 22.95° (114), 25.59° (002), 40.54° (200), 70.46° (311) [122-124]. Peaks at 40.54° and 70.46° corresponds to MnO [127-129]. In specifically, the presence of rGO can be determined by the existence of a 2 peak with a low intensity located at 25.59° (002) (CCDC no. #671073) [125]. The XRD examination has yielded fruitful data regarding the successful creation

of the intended nanocomposite consisting of rGO, Mn and ZIF-67.

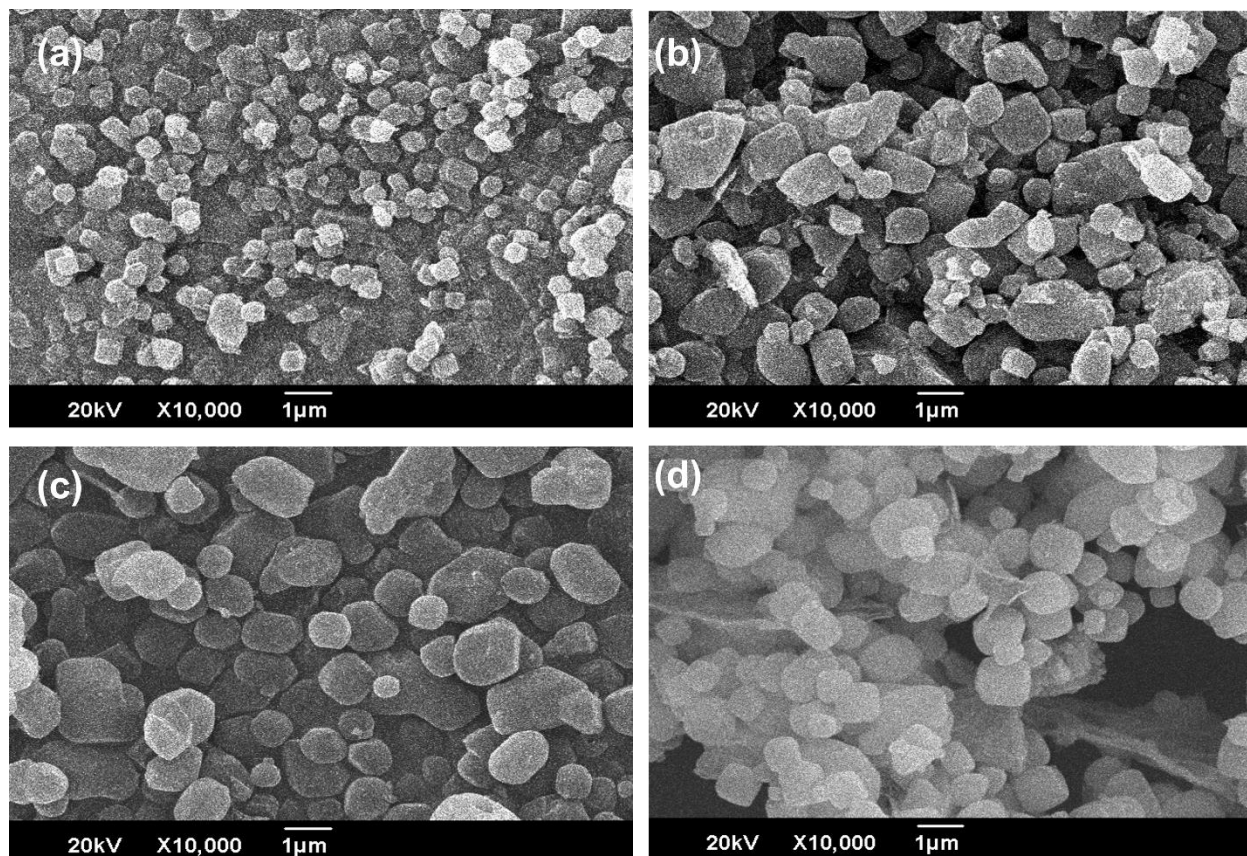


Figure 7: SEM image of a) ZIF-67, b) 1wt% rGO/ZIF-67, c) 3wt% rGO/ZIF-67, d) 5wt% rGO/ZIF-67

The scanning electron microscope gives magnified images of the shape, size, crystallography, composition, and other chemical and physical properties of the material. Figure 7 (a-d) represents the SEM images of ZIF-67 and its composite with rGO. ZIF-67 in the image shows a hexahedral structure. The sheets of rGO are completely visible in the SEM images, indicating the successful incorporation of rGO in ZIF-67 structure. The rGO sheets increased the dispersibility of ZIF-67 [130]. The morphological and microstructural investigations with SEM reveal that the proposed strategy to synthesize the ZIF-67/rGO composite has resulted in the development of the intended composite wherein the structural features of both the components were able to be preserved. This conclusion is supported by the fact that the formation of the composite was brought about because of the formation of the desired composite. It was essential to accomplish this in order to guarantee the effective storage of charge via an increase in the electrolyte ion movement within the electrode

material [131]. Because ZIF-67 is present, greater porosity is created, which should make it easier for the electrode material to have high performance.

Energy dispersive X-Ray spectroscopy for elemental analysis is used as a characterization technique. It shows the successful preparation of our composite material. The hybridized material consists of Carbon, Nitrogen, Oxygen and Co, their compositions are given in table 2. It tells us that the prepared samples only contain desired constituents in the synthesized desired catalyst. EDX table shows that the desired rGO/ZIF-67 was successfully prepared by sol-gel method.

Table 2: Energy Dispersive X-Ray Spectroscopy

Element	ZIF-67	1 wt% rGO/ZIF-67	3 wt% rGO/ZIF-67	5 wt% rGO/ZIF-67
C	35.2	37.4	40.2	42.1
N	20.1	19.5	17.4	18.3
O	21.2	20.4	20.7	19.1
Co	23.5	22.7	21.7	20.5

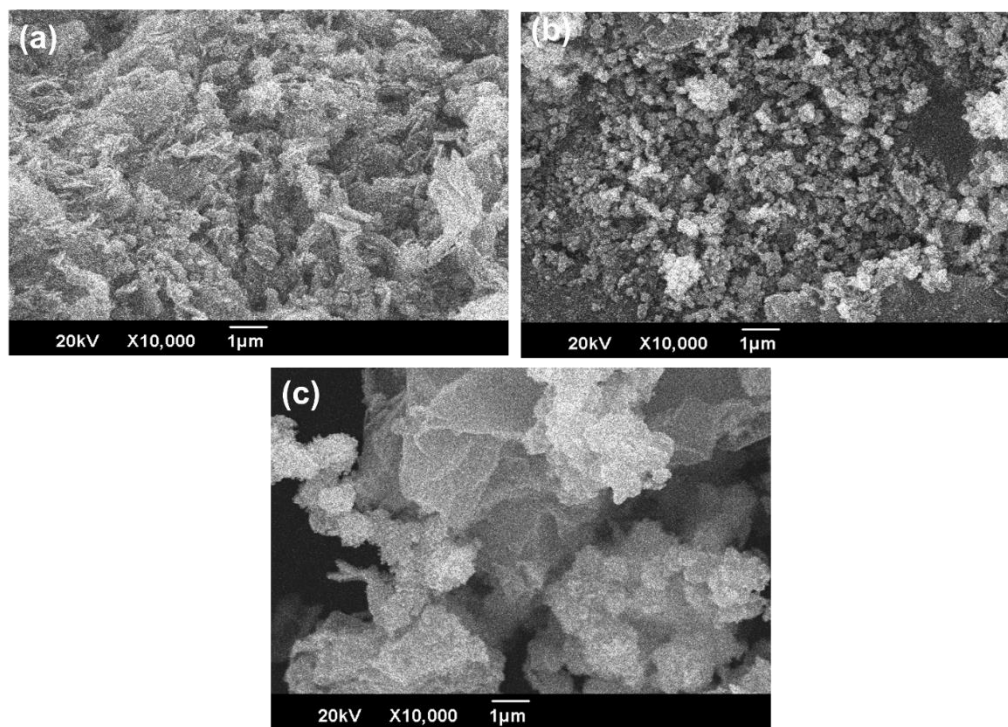


Figure 8: SEM image of a) 1 wt% rGO/Mn ZIF-67 b) 3 wt% rGO/Mn ZIF-67 c) 5 wt% rGO/Mn ZIF-67

Figure 8 shows SEM images of 1, 3, 5 wt% rGO/Mn ZIF-67. Figure show the SEM image of Mn-ZIF-67 which were nanoparticles. The composite surface became blocky and showed crystals of Mn-ZIF67 which were loaded on the surface of rGO sheets. Mn-ZIF-67 are crystalline in nature and rGO has sheets. The sheets of rGO are completely visible in the SEM images, indicating the successful incorporation of rGO in ZIF-67 structure. The rGO sheets increased the dispersibility of ZIF-67 [130]. The morphological and microstructural investigations with SEM reveal that the proposed strategy to synthesize the ZIF-67/rGO composite has resulted in the development of the intended composite wherein the structural features of both the components were able to be preserved. This conclusion is supported by the fact that the formation of the composite was brought about because of the formation of the desired composite. It was essential to accomplish this in order to guarantee the effective storage of charge via an increase in the electrolyte ion movement within the electrode material [131]. Because ZIF-67 is present, greater porosity is created, which should make it easier for the electrode material to have high performance.

The composite material provides higher surface area and provides more active sites as a catalyst material. The obtained catalyst electrochemical activity is enhanced by this morphology.

Table 3. shows the EDX analysis of 1, 3, 5 wt% rGO/Mn ZIF-67. The composite material is composed of carbon, nitrogen, oxygen, cobalt, and manganese. These compositions indicate the successful preparation of our composite material without any impurity resulting in higher activity as a catalyst.

Table 3: Energy Dispersive X-Ray Spectroscopy

Element	1 wt% rGO/Mn ZIF-67	3 wt% rGO/Mn ZIF-67	5 wt% rGO/Mn ZIF-67
C	22.4	25.1	29.2
N	20.1	16.5	15.8
O	17.8	17.8	16.3
Co	19.3	19.5	20.4
Mn	20.4	21.1	18.3

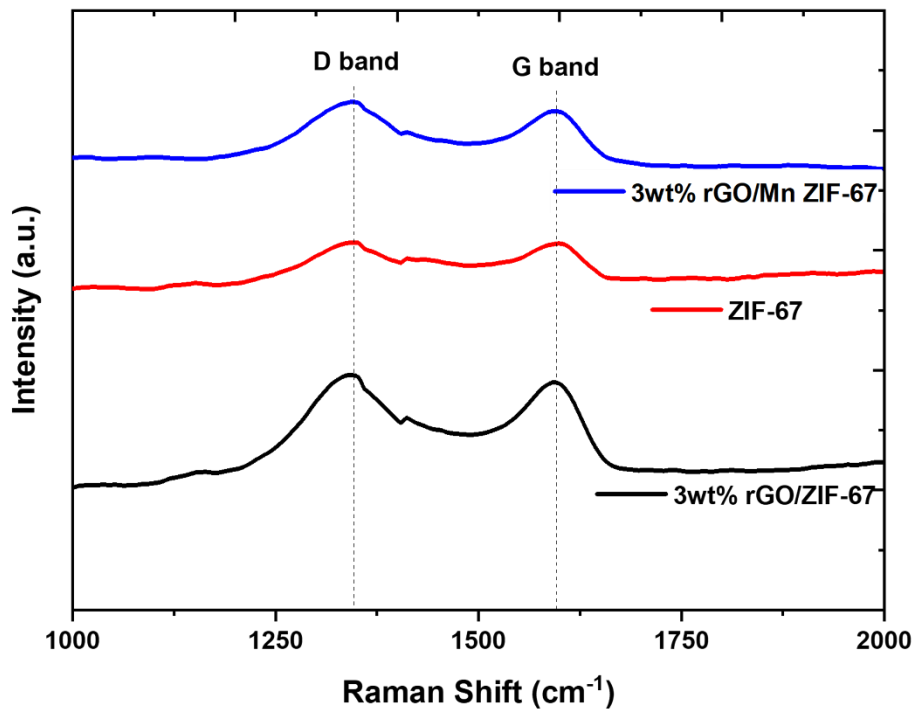


Figure 9: Raman spectroscopy of ZIF-67, 3wt% rGO/ZIF-67, 3wt% rGO/Mn ZIF-67

The vibrational modes of the samples under investigation have been analyzed with the use of Raman spectroscopy (Fig. 9). These investigations were carried out within a spectral band spanning 400–4000 cm⁻¹ at settings corresponding to room temperature (RT). The ZIF-67/rGO sample was analyzed, and the results showed that it had two strong peaks at 1349 and 1579 cm⁻¹, which were connected with the D and G bands of rGO nanosheets, respectively [132]. It is common knowledge that the D band is present in all sp² hybridized carbon lattices and that its presence correlates with the stretching of C–C bonds. A second sign of defect- and disorder-induced breathing pattern of sp² rings can be found in the D band [132]. Presence of flaws in rGO fraction was indicated by fact that intensity of D band was higher than the intensity of the G band. These defects could have been introduced during chemical reduction stage.

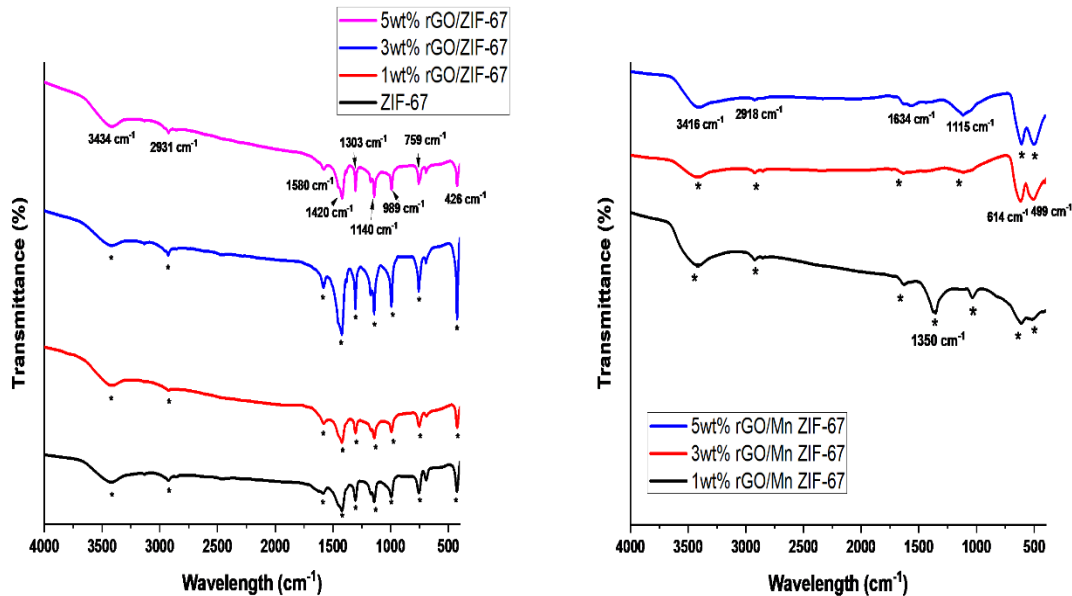


Figure 10: FTIR a) ZIF-67, 1wt% rGO/ZIF-67, 3wt% rGO/ZIF-67, 5wt% rGO/ZIF-67 b) 1wt% rGO/Mn ZIF-67, 3wt% rGO/Mn ZIF-67, 5wt% rGO/Mn ZIF-67

Figure 10 illustrates the Fourier transform infrared (FTIR) spectra of ZIF-67 and ZIF-67/rGO. A band with a frequency of around 3434 cm^{-1} was found to be shared by the two samples. This band was interpreted to represent the surface O-H stretching vibrations of the C-OH group [123]. The reduction of GO into rGO was verified by a strong band at 1634 cm^{-1} , which is related to epoxide and was observed in the rGO sample. This band was located at the same frequency as epoxide. In addition, the skeletal vibration of rGO was responsible for observing a band with a lower intensity located at 1634 cm^{-1} . There was no substantial signal seen that was linked with (nonreduced) graphene oxide (GO) [for example, at 1040 cm^{-1} (C-OC), 1621 cm^{-1} (C=O), 1732 cm^{-1} (C=O), 3400 cm^{-1} (OH), 1415 cm^{-1} (C-O-H), 1220 cm^{-1} (C-O)] to indicate presence of graphene as reduced graphene oxide (rGO). Frequencies of 759, 989, 1140, 1303, 1420, and 1580 cm^{-1} were identified as being associated with the ZIF-67 bands [122, 133]. A band at 499 cm^{-1} represents the presence of metal oxides (MnO_x). The bands detected in the range between 600 and 1502 cm^{-1} related to the stretching and bending modes of ZIF-67. On the other hand, a particular signal detected at 1580 cm^{-1} may be linked to stretching modes of C=C and C=N [134]. Evidence that 1-5 wt% rGO/ZIF-67 composite was successfully formed was supplied by distinctive signals originating from both rGO and ZIF-67.

4.2 Electrocatalytic Measurements

4.2.1 Preparation of ZIF 67 Electrode

The substrate used for ZIF 67 electrode preparation is Ni. Preparation of ZIF 67 electrode consists of two steps. In the first step, the Ni foam is treated. Ni foam (NF) is added to the solution of 4 ml HCl and 40 ml of DI water, which is sonicated for 35 mins. Then the NF is added to 20 ml ethanol and sonicated for 25 mins. NF is again sonicated for 25 mins in DI water. In the second step, 5-7 mg of catalyst is added to 0.68 ml of ethanol and stirred till the solution becomes uniform; after that, 3 drops of Nafion are added and stirred for 5 mins. NF is added to ink solution and stirred for 25 mins. Then the solution is dried at 40°C. ZIF 67 electrode is prepared, and the same procedure is repeated for ZIF67 and its composites.

4.2.2 OER

To perform electrocatalytic studies by chronopotentiometry, EIS, LSV, and CV tests; NF has been used as an electrode. A three-electrode assembly consisting of three electrodes is required to conduct electrocatalytic tests. First electrode is Pt wire, which is used as counter electrode; second electrode is our working electrode which consists of our catalyst deposited on Ni foam. Third one is reference electrode, which is usually Ag/AgCl. 1 M KOH solution is used as an electrolyte. The reference electrode and the working electrode both have a voltage applied to them. The OER is driven by this voltage, which also enables accurate measurement of the current that is moving through the system. The electrochemical kinetics of the OER, including the reaction rate, catalytic efficiency, and overpotential, can be investigated by altering the voltage that is supplied and then monitoring the current that is produced because of this manipulation. Higher catalytic efficiency can be achieved when the potential of the electrocatalyst is increased in tandem with its rate of reaction [67]. There are four stages involved in this OER mechanism reaction [66].

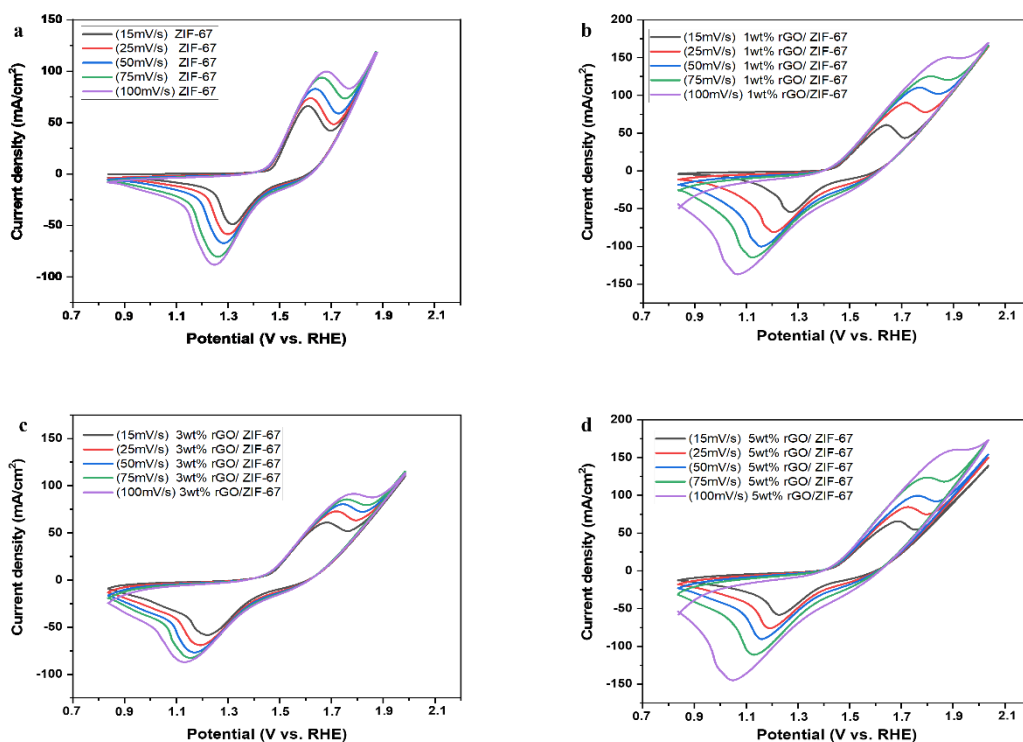


Figure 11: Cyclic voltammetry plots at 15, 25, 50, 75, 100 mV/s scan rate of a) ZIF-67 b) 1wt% rGO/ZIF-67 c) 3wt% rGO/ZIF-67 d) 5wt% rGO/ZIF-67

Cyclic voltammetry, often known as CV, is an electrochemical technique that is used to analyze electrochemical behavior of an electrode, research the redox properties of a system, and acquire information regarding reaction kinetics, electron transport mechanisms, and surface activities. It includes measuring the current that is produced by an electrochemical cell while a potential sweep is being applied to the cell. To understand scan rate and current density better, cyclic voltammetry is usually performed. The cyclic voltametric plots of ZIF-67, and 1-5 wt% rGO/ZIF-67 are shown in Fig. 11 (a-d). The CV plots were studied at scan rates of 15, 25, 50, 75, and 100 mV/s. At 15 mV/s scan rate the value of current density oxidation peak for ZIF-67, 1wt% rGO/ZIF-67, 3wt% rGO/ZIF-67, and 5wt% rGO/ZIF-67 are 60.02 mAcm^{-2} , 61.01 mAcm^{-2} , 64.17 mAcm^{-2} , and 62.3 mAcm^{-2} . The current density reduction peak for ZIF-67, 1wt% rGO/ZIF-67, 3wt% rGO/ZIF-67, and 5wt% rGO/ZIF-67 are -48.69 mAcm^{-2} , -54.57 mAcm^{-2} , -58.3 mAcm^{-2} , and -55.82 mAcm^{-2} . The enhanced currents in rGO/ZIF-67 when compared to ZIF-67 were attributed to composite electrode's rising electrical conductivity and accessible active sites, both of which led to an increase

in the rate of ion diffusion and electron transfer through composite electrode. This was demonstrated by a comparison of the two electrodes [126, 135]. As the scan rate increases, the diffusion rate also increases as a result the value of current oxidation peaks increases.

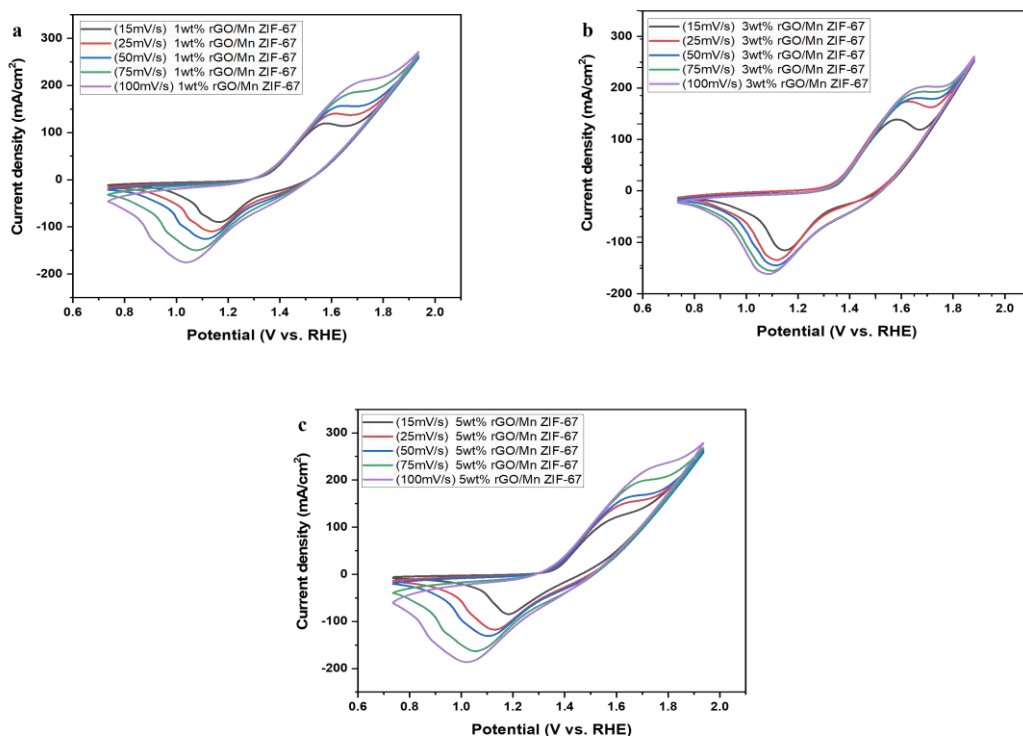


Figure 12: Cyclic voltammetry plots at 15, 25, 50, 75, 100 mV/s scan rate of a) 1wt% rGO/Mn ZIF-67 b) 3wt% rGO/Mn ZIF-67 c) 5wt% rGO/Mn ZIF-67

The cyclic voltametric plots of 1-5 wt% rGO/ZIF-67 are shown in Fig. 12 (a-c). The CV plots were studied at scan rates of 15, 25, 50, 75, and 100 mV/s. At 15 mV/s scan rate value of current density oxidation peak for 1wt% rGO/Mn ZIF-67, 3wt% rGO/Mn ZIF-67, and 5wt% rGO/Mn ZIF-67 are 121.4 mAcm^{-2} , 138.7 mAcm^{-2} , and 119.3 mAcm^{-2} . The current density reduction peak for 1wt% rGO/Mn ZIF-67, 3wt% rGO/Mn ZIF-67, and 5wt% rGO/Mn ZIF-67 are -85.33 mAcm^{-2} , -115.1 mAcm^{-2} , and -89.5 mAcm^{-2} . Porous carbon framework not only raises the electrical conductivity but also makes it easier for ions and oxygen to move around, which ultimately leads to an improvement in the material's bifunctional activity [136].

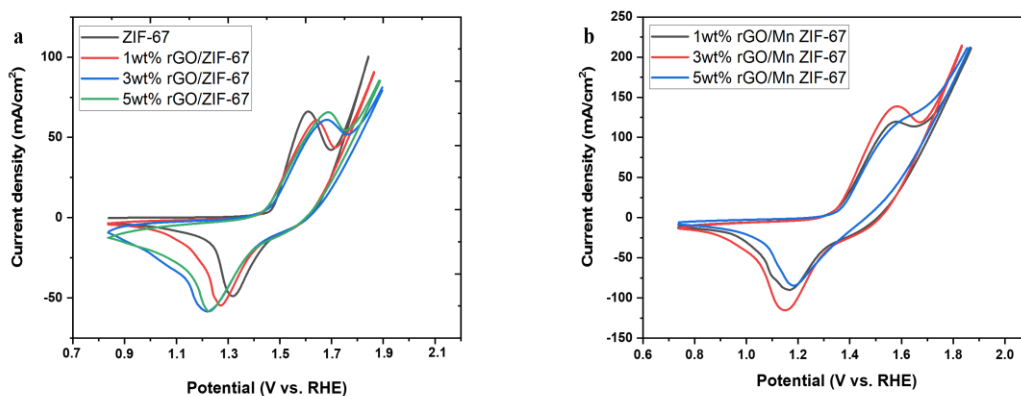


Figure 13: Combined Cyclic voltammetry plots a) ZIF-67, 1wt% rGO/ZIF-67, 3wt% rGO/ZIF-67, 5wt% rGO/ZIF-67 b) 1wt% rGO/Mn ZIF-67, 3wt% rGO/Mn ZIF-67, 5wt% rGO/Mn ZIF-67

Fig. 13 (a, b) shows combined CV curves of ZIF-67, 1wt% rGO/ZIF-67, 3wt% rGO/ZIF-67, 5wt% rGO/ZIF-67 b) 1wt% rGO/Mn ZIF-67, 3wt% rGO/Mn ZIF-67, and 5wt% rGO/Mn ZIF-67. It shows by combining ZIF-67 with rGO the values of current density oxidation peaks increases because rGO possess excellent chemical and mechanical stability, good electrical conductivity, and high surface area[137, 138]. Also, by introducing MnO₂, the values of current oxidation peaks increased. The following is a list of the MnO_x that are responsible for extraordinary efficiency of catalyst: (1) increased charge transfer and a decrease in the batteries' internal resistance due to direct contact between catalyst and electrode (2) the catalyst helped prevent detachment and agglomeration caused by direct growth on the electrode. (3) the electrolyte and oxygen both make direct contact with porous structure of the air cathode. Due to the simplicity with which one can gain access to electroactive surface area, the resulting response throughout the charge-discharge cycle is both reliable and consistent [139]. As we can see from the figure the reduction peak is being shifted to lower values due to addition of rGO. rGO is an extremely conductive substance that has a huge surface area, which makes it easier for electrons to move quickly and efficiently. When rGO is combined with ZIF-67, a conductive network is produced, which results in an increase in composite material's capacity to transmit electrical current. This improved capacity for the transfer of electrons makes it possible to have reduction reactions that are both faster and more efficient, which causes a change in the peak potential of the reduction to a lower value. The overall electroactive surface area of the composite material is increased when rGO is included in the ZIF-

67 formulation. Due to the increased surface area, there are now more active locations where redox reactions can take place. Consequently, during the reduction process, a greater number of electrochemical processes take place, which results in a stronger current responsiveness at lower potentials. It's possible that the presence of rGO in the composite material will let the ions move more freely throughout the electrode. Because of the increased ion diffusion, it is now possible to move reactants to the electrode surface more quickly, which in turn leads to more effective reduction processes. The decreased resistance of the electrochemical process that is brought about by the facilitation of ion diffusion brings about a movement of the reduction peak to lower potentials. When coupled, rGO and ZIF-67 have the potential to demonstrate synergistic effects. This refers to a situation in which the properties of both individual components are improved because of their combination. Because of the interaction between rGO and ZIF-67, charge transport can be improved, the number of electroactive sites can be increased, and the level of catalytic activity can be increased; all these factors contribute to a shift in the reduction peak toward lower potentials. As a transition metal, manganese (Mn) can undergo redox processes, which include the alteration of its oxidation state. There are now redox-active species present in the system because of the addition of Mn to ZIF-67. Mn species have the potential to take part in electron transfer processes during the reduction process, which can ultimately result in the reduction of Mn ions. This increased redox activity leads to the reduction peak shifting to lower potentials, which adds to the peak's formation. Additionally, Mn can play the role of a catalyst, which enables it to speed up reduction reactions within the system. It has the potential to offer up extra active sites for electron transfer and boost the catalytic performance of ZIF-67. Because Mn is present, the efficiency of the reduction reactions is improved, which results in a greater current response at lower potentials and causes the reduction peak to shift to lower potentials. The inclusion of Mn has the potential to cause changes to the electrochemical environment of ZIF-67. Mn ions can have interactions with the framework, change the local electronic structure, and adjust the redox characteristics of the material. These alterations can affect the kinetics of the reduction process, which will result in a movement of the reduction peak toward lower potentials. The addition of Mn to ZIF-67 has the potential to cause modifications to occur in the electronic structure of the composite material. The amount of energy needed to complete the reduction process can be affected by Mn's ability to either introduce new energy levels or modify the

structure of the energy band. Because of this alteration in the electrical structure, there is a possibility that the reduction peak will move to lower potentials.

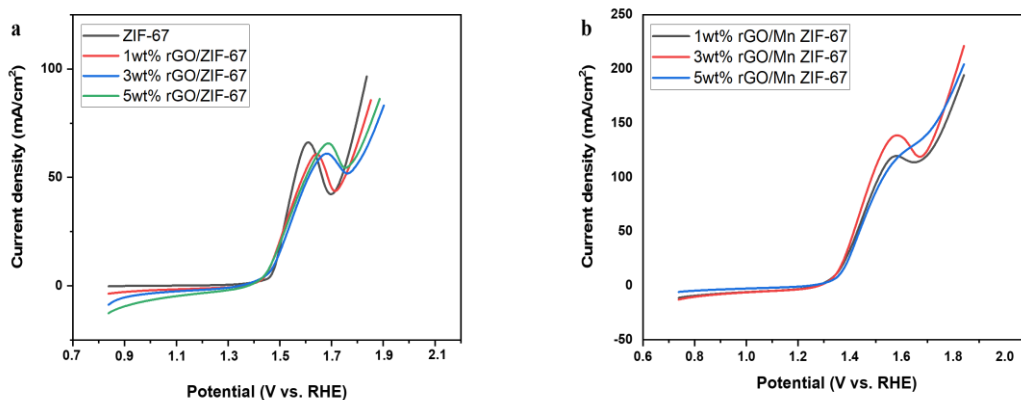


Figure 14: LSV plots a) 1wt% rGO/Mn ZIF-67, 3wt% rGO/Mn ZIF-67, 5wt% rGO/Mn ZIF-67 b) ZIF-67, 1wt% rGO/ZIF-67, 3wt% rGO/ZIF-67, 5wt% rGO/ZIF-67

A technique known as linear sweep voltammetry, or LSV, is an electrochemical method that is used to analyze the redox behavior of a system and monitor the electrochemical reactions that take place at an electrode. A linear potential sweep is delivered to the working electrode during LSV, and the resulting current is measured during the process. An experiment called an LSV involves continually sweeping a potential in a linear fashion with either time or scan rate. In most cases, the potential will be swept either from its initial potential to its end potential or vice versa. It is possible to measure the resulting current as a function of the potential that has been applied. The polarization curve of LSV is used to check the OER performance of hybrid material. Catalysts were analyzed under the same conditions, to find out the effect of Mn, rGO over ZIF-67. Fig. 14 (a, b) shows OER's polarization curves. LSV represents the difference between 1wt% rGO/Mn ZIF-67, 3wt% rGO/Mn ZIF-67, 5wt% rGO/Mn ZIF-67, ZIF-67, 1wt% rGO/ZIF-67, 3wt% rGO/ZIF-67, and 5wt% rGO/ZIF-67. To find the OER performance, overpotential of catalyst is determined. Overpotential is calculated by $E - E_0$ [140]. As can be seen in Fig. 13 (a, b), value of 10 mAcm^{-2} is used to determine the overpotential. The over potential value of 1wt% rGO/Mn ZIF-67, 3wt% rGO/Mn ZIF-67, 5wt% rGO/Mn ZIF-67, ZIF-67, 1wt% rGO/ZIF-67, 3wt% rGO/ZIF-67, and 5wt% rGO/ZIF-67 are 131, 113, 115, 279, 268, 259, and 267 mV respectively. 3wt%

rGO/Mn ZIF-67 only needs 113 mV overpotential, as compared to ZIF-67 which large overpotential of 279 mV.

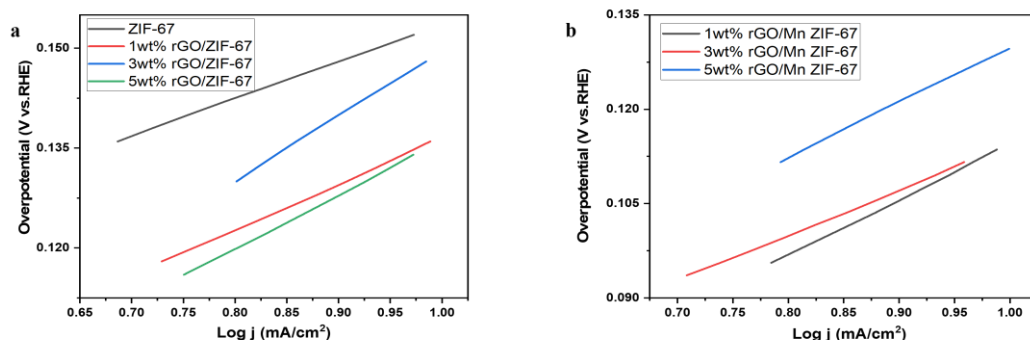


Figure 15: Tafel slope a) ZIF-67, 1wt% rGO/ZIF-67, 3wt% rGO/ZIF-67, 5wt% rGO/ZIF-67 b) 1wt% rGO/Mn ZIF-67, 3wt% rGO/Mn ZIF-67, 5wt% rGO/Mn ZIF-67

The slope of the Tafel plot is connected to the reaction mechanism as well as the step in the electrochemical reaction that determines the rate. The kinetics and electrochemical behavior of the system can be better understood because of this finding. The slope of the Tafel can be affected by a variety of parameters, such as the composition of the electrode material, the mechanism of the reaction, the number of reactants present, and the existence of catalysts. The interpretation of the Tafel slope shows that a more efficient electrochemical reaction with faster kinetics is associated with a smaller Tafel slope, whereas a bigger Tafel slope is associated with a slower reaction kinetics. The slope of the Tafel can also give information on the mechanism of charge transfer, the nature of the electrochemical process (such as whether it is governed by diffusion or adsorption), and the existence of reaction intermediates. Electrocatalyst' Tafel slopes are represented in Fig. 15 (a, b). The tafel slope values of 1wt% rGO/Mn ZIF-67, 3wt% rGO/Mn ZIF-67, 5wt% rGO/Mn ZIF-67, ZIF-67, 1wt% rGO/ZIF-67, 3wt% rGO/ZIF-67, and 5wt% rGO/ZIF-67 are 71.0, 55.0, 69.0, 97.7, 88.2, 80.3, and 87.8 mV/dec⁻¹ respectively. 3wt% rGO/Mn ZIF-67 showed lowest value of tafel slope (55.0 mV/dec⁻¹) among prepared catalysts. In comparison, ZIF-67 offers the highest value (97.7 mV/dec⁻¹) among prepared catalysts because of high resistance in charge transportation. Addition of Mn and rGO causes the values of tafel slope to decrease. The presence of Mn and rGO results in the introduction of new redox-active species into the system. As a transition metal, Mn can undergo redox processes, which include the alteration of its oxidation

state. In a similar manner, rGO possesses electronic conductivity and can participate in processes involving electron transfer. Because these redox-active species are present, there are more active sites available for electrochemical reactions; therefore, reaction kinetics are increased, and the electrochemical process is carried out more effectively. Mn and rGO both contribute to an increase in the composite material's ability to conduct electricity. Within the electrode material, the presence of Mn ions and rGO sheets combine to form a conductive network that makes it easier for charge carriers, like electrons, to move around. Due to the increase in conductivity, there is a faster movement of electrons between the redox-active species and the electrode surface, which results in a flatter Tafel slope. They were able to change the surface characteristics as well as the electrochemical environment of ZIF-67. Interactions between Mn ions and rGO sheets and the ZIF-67 framework can result in modifications to the framework's electronic structure and an increase in its catalytic activity. These alterations make it easier for reactant species to adsorb and get activated at the electrode surface, which in turn makes the electrochemical reactions go more smoothly and results in a flatter Tafel slope.

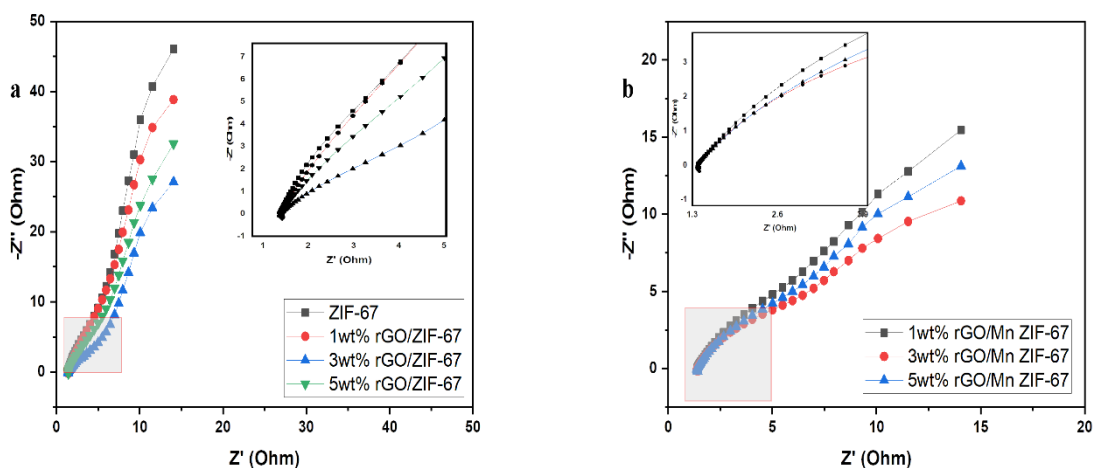


Figure 16: EIS plots a) 1wt% rGO/Mn ZIF-67, 3wt% rGO/Mn ZIF-67, 5wt% rGO/Mn ZIF-67 b) ZIF-67, 1wt% rGO/ZIF-67, 3wt% rGO/ZIF-67, 5wt% rGO/ZIF-67

To check the catalyst capacitance and resistance properties, electrochemical impedance spectroscopy (EIS) is used. The capacitance and resistance values are determined by measuring current out-phase and in-phase responses. At the cathode and anode, the electrochemical reactions

occurring is provided by EIS. To learn how catalyst performed after it was synthesized was made by EIS measurement [141]. In Fig. 16(a, b), the EIS representation is shown. The main purpose is to find resistance by EIS [142]. The EIS plot is shown by Nyquist plot, at the electrode surface it is used to find resistance from faradic reaction [143]. It can be deduced from the EIS plots that 5wt% rGO/Mn ZIF-67 shows low value of 9.613 Ω charge transfer resistance (R_{ct}), that is represented by semi-circle of less diameter, which indicates how good the charge can be moved. Electrolyte resistance of 1wt% rGO/Mn ZIF-67, 3wt% rGO/Mn ZIF-67, 5wt% rGO/Mn ZIF-67, ZIF-67, 1wt% rGO/ZIF-67, 3wt% rGO/ZIF-67, and 5wt% rGO/ZIF-67 values are 1.385 Ω , 1.491 Ω , 1.382 Ω , 2.749 Ω , 1.798 Ω , 1.564 Ω , and 1.422 Ω respectively. The decrease in diameter of semi-circle, shows resistance values lower, which represents catalyst's charge transfer rate higher [143, 144]. The highly conductive rGO makes it easier for electrons to move across the composite and for ions to diffuse into the redox sites. This results in an increase in the electrical conductivity of rGO/ZIF-67 in comparison to the electrical conductivity of naked ZIF-67. Furthermore, ZIF-67 particles have a propensity to agglomerate. The incorporation of rGO into the MOF substrate, on the other hand, caused ZIF-67 particles to become more dispersed, which contributed to an increase in the capacitance of the composite electrode material [126, 145]

Table 4: R_u , C_f , and R_{ct} values of synthesized catalysts in this study

Sr. no.	Catalyst	R_{ct} (ohm)	R_u (ohm)	C_f (Farad)
1	ZIF-67	62.84	2.749	1.418e ⁻³
2	1wt% rGO/ZIF-67	47.58	1.798	3.501 e ⁻³
3	3wt% rGO/ZIF-67	38.95	1.564	1.239 e ⁻³
4	5wt% rGO/ZIF-67	33.95	1.422	1.675 e ⁻³
5	1wt% rGO/Mn ZIF-67	12.93	1.385	1.637 e ⁻³
6	3wt% rGO/ Mn ZIF-67	9.613	1.382	1.779 e ⁻³
7	5wt% rGO/ Mn ZIF-67	11.32	1.491	1.817 e ⁻³

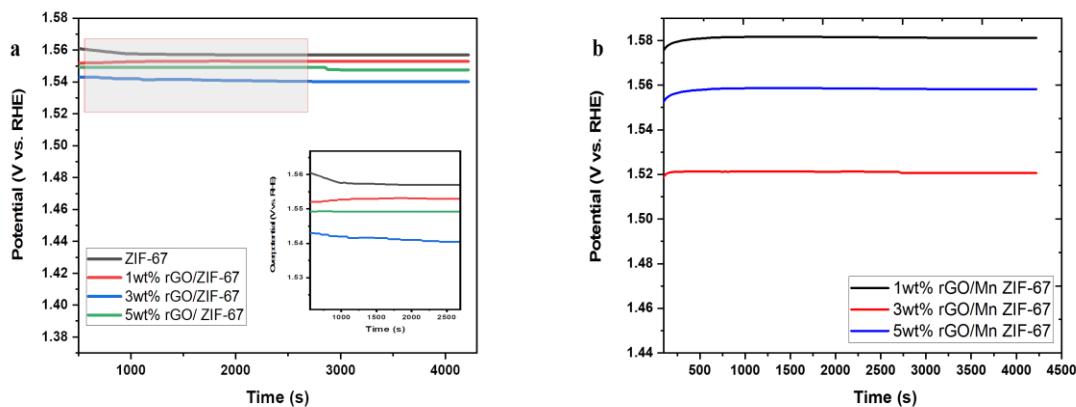


Figure 17: Chronopotentiometry a) 1wt% rGO/Mn ZIF-67, 3wt% rGO/Mn ZIF-67, 5wt% rGO/Mn ZIF-67 b) ZIF-67, 1wt% rGO/ZIF-67, 3wt% rGO/ZIF-67, 5wt% rGO/ZIF-67

Chronopotentiometry is a technique that is used in electrochemistry to measure the change in potential of an electrode as a function of time while a constant applied current is being applied. During this procedure, a steady current is passed through the working electrode, and the subsequent potential response is monitored and recorded over the course of time. Electrocatalyst stability is an important parameter for OER. This can be measured by altering linear sweep voltammetry over 1000 CV scan. Also, by durability test it can be depicted, which is provided by adjusting the performance at one applied potential or specific current density with respect to time. As can be seen in Fig. 18, the stability of 3wt% rGO/Mn ZIF-67 was determined at 10mA for one hour. The result shows the consistent behavior throughout one hour of the prepared catalyst which can be due to the structure of the catalyst. It is a lot easier for ions to move across active sites which are exposed due to low resistance of ion diffusion. At the start of the chronopotentiometry test, there is a rapid change but with time, there is no change. The result shows that the catalyst is stable.

Conclusion

This study centered on the application of ZIF-67 and its composites, specifically 1-5wt% rGO/ZIF-67 and 1-5wt% rGO/Mn ZIF-67, as electrocatalysts in metal-air batteries for the oxygen evolution reaction (OER). The purpose of the study was to investigate the sluggish OER kinetics that impair the overall performance of metal-air batteries, with the goal of proposing alternative solutions for boosting the efficiency and use of these batteries.

The outcomes of the research showed some promising results, which were discovered through the synthesis and characterization of ZIF-67 and its composites. The catalytic activity and stability of the electrocatalysts that were produced because of incorporating reduced graphene oxide (rGO) and manganese (Mn) into the ZIF-67 structure was greatly improved. The additive actions of rGO and Mn resulted in a facilitated electron transfer and the provision of extra active sites for the OER, both of which contributed to an improvement in performance.

The electrochemical experiments revealed that the ZIF-67-derived electrocatalysts exhibited improved OER performance when compared to the performance of traditional catalysts. The overpotential values for ZIF-67 were calculated as 154mV at 10 mAcm⁻². By the addition of rGO, overpotential values were reduced. The optimum addition of rGO was 3wt% as it gave an overpotential value of 136mV 10 mAcm⁻². The addition of 5wt% rGO caused the blockage of active sites. The addition of Mn significantly improved the activity of ZIF-67. 3wt% rGO/Mn ZIF-67 outperformed all the compositions of catalysts being performed in this study, with an overpotential value of 113 mV at 10 mAcm⁻². These findings highlight the potential of ZIF-67 and its composites as efficient electrocatalysts for metal-air batteries. By resolving the issues associated with the oxygen electrode and opening up new possibilities for the practical application of these batteries, the challenges that are associated with the oxygen electrode can be overcome.

The findings of the research that are described in this thesis contribute important new insights into the development and synthesis of electrocatalysts for MAB, with particular emphasis on OER. The research and development compounds based on ZIF-67, in addition to their composites, provides a significant opportunity for making headway in the field of environmentally friendly energy storage technologies. It is possible that additional research and tuning of these electrocatalysts will

lead to even more substantial breakthroughs in the performance of metal-air batteries. This will get us closer to achieving their full potential as energy storage systems that are both environmentally benign and have a high energy density.

In the end, the findings from this research study contribute to the overarching objective of attaining a sustainable and low-carbon future by decreasing reliance on fossil fuel; accelerating development of clean energy technology. The use of ZIF-67 and its composites in metal-air batteries represents a significant step forward in addressing the challenges of the oxygen electrode. This paves the way for the practical application of metal-air batteries in a variety of fields, including the integration of renewable energy, grid-scale energy storage, and electric transportation, among other applications.

Future Recommendations

Following are some suggestions for more study and development in ZIF-67 derived electrocatalysts for use as the oxygen electrode in metal-air batteries, which may be made based on the findings and conclusions presented in this thesis:

1. **Prolonged Stability tests:** It is essential for the practical application of ZIF-67 derived electrocatalysts in metal-air batteries to conduct research on the long-term stability and endurance of these electrocatalysts. The results of experiments involving extended cycling and accelerated aging that are carried out under conditions that are representative of actual working environments would provide significant information regarding the performance deterioration of the catalyst, as well as viable solutions for increasing its stability.
2. **Catalyst Design and Engineering:** Catalytic activity and stability of ZIF-67 derived electrocatalysts can be further improved by exploring fresh methods of catalyst engineering and design. These methods include the controlled synthesis of hierarchical structures, doping with a variety of elements, and surface modification. Computational modeling and simulation studies have the potential to provide beneficial insights into the catalytic mechanisms and help the rational design of new catalysts.
3. **Integration and scale-up:** It is necessary to put these electrocatalysts into practical use, to investigate manufacturing procedures that can be scaled up and to find ways to increase the yield of their synthesis methods. In addition, it will be necessary to integrate these electrocatalysts into functioning electrode structures and whole metal-air battery systems to evaluate their performance in real-world applications and determine whether they are compatible with the other components of the battery.
4. **Composite Structure's Optimization:** Even though the integration of manganese and reduced graphene oxide into ZIF-67 demonstrated encouraging results, there is still potential for future improvement of the composite structures. Exploring a variety of alternative material ratios and combinations has the potential to result in electrocatalysts with improved catalytic performance, increased stability, and increased overall efficiency.

5. Optimization of the system: Future research should concentrate on perfecting the design of the metal-air battery, including the anode, electrolyte, and all the other components of the battery. This is important when considering the larger system-level optimization. If the synergistic effects of the ZIF-67 derived electrocatalyst and other materials within the battery system are investigated, it is possible that this will lead to further improvements in energy efficiency, performance, and the overall battery longevity.

References

- [1] A. Banerjee, K. E. Halvorsen, A. Eastmond-Spencer, and S. R. Sweitz, "Sustainable development for whom and how? Exploring the gaps between popular discourses and ground reality using the Mexican *Jatropha* biodiesel case," *Environmental management*, vol. 59, pp. 912-923, 2017.
- [2] B. Huskinson *et al.*, "A metal-free organic–inorganic aqueous flow battery," *Nature*, vol. 505, no. 7482, pp. 195-198, 2014.
- [3] H. Li *et al.*, "Enhanced ferroelectric-nanocrystal-based hybrid photocatalysis by ultrasonic-wave-generated piezophototronic effect," *Nano letters*, vol. 15, no. 4, pp. 2372-2379, 2015.
- [4] S. W. Kim, D. H. Seo, X. Ma, G. Ceder, and K. Kang, "Electrode materials for rechargeable sodium-ion batteries: potential alternatives to current lithium-ion batteries," *Advanced Energy Materials*, vol. 2, no. 7, pp. 710-721, 2012.
- [5] X. Yu *et al.*, "Hierarchical TiO₂ nanowire/graphite fiber photoelectrocatalysis setup powered by a wind-driven nanogenerator: A highly efficient photoelectrocatalytic device entirely based on renewable energy," *Nano Energy*, vol. 11, pp. 19-27, 2015.
- [6] J. Suntivich, H. A. Gasteiger, N. Yabuuchi, H. Nakanishi, J. B. Goodenough, and Y. Shao-Horn, "Design principles for oxygen-reduction activity on perovskite oxide catalysts for fuel cells and metal–air batteries," *Nature chemistry*, vol. 3, no. 7, pp. 546-550, 2011.
- [7] P. G. Bruce, S. A. Freunberger, L. J. Hardwick, and J.-M. Tarascon, "Li–O₂ and Li–S batteries with high energy storage," *Nature materials*, vol. 11, no. 1, pp. 19-29, 2012.
- [8] M. K. Debe, "Electrocatalyst approaches and challenges for automotive fuel cells," *Nature*, vol. 486, no. 7401, pp. 43-51, 2012.
- [9] G. Wu and P. Zelenay, "Nanostructured nonprecious metal catalysts for oxygen reduction reaction," *Accounts of chemical research*, vol. 46, no. 8, pp. 1878-1889, 2013.
- [10] R. Borup *et al.*, "Scientific aspects of polymer electrolyte fuel cell durability and degradation," *Chemical reviews*, vol. 107, no. 10, pp. 3904-3951, 2007.
- [11] J. C. Meier *et al.*, "Stability investigations of electrocatalysts on the nanoscale," *Energy & Environmental Science*, vol. 5, no. 11, pp. 9319-9330, 2012.

- [12] Q. Li, R. Cao, J. Cho, and G. Wu, "Nanocarbon electrocatalysts for oxygen reduction in alkaline media for advanced energy conversion and storage," *Advanced energy materials*, vol. 4, no. 6, p. 1301415, 2014.
- [13] Y. Liang *et al.*, "Co₃O₄ nanocrystals on graphene as a synergistic catalyst for oxygen reduction reaction," *Nature materials*, vol. 10, no. 10, pp. 780-786, 2011.
- [14] S. Yang, X. Feng, X. Wang, and K. Müllen, "Graphene-based carbon nitride nanosheets as efficient metal-free electrocatalysts for oxygen reduction reactions," *Angewandte Chemie International Edition*, vol. 50, no. 23, pp. 5339-5343, 2011.
- [15] T. Y. Ma, S. Dai, M. Jaroniec, and S. Z. Qiao, "Graphitic carbon nitride nanosheet-carbon nanotube three-dimensional porous composites as high-performance oxygen evolution electrocatalysts," *Angewandte Chemie*, vol. 126, no. 28, pp. 7409-7413, 2014.
- [16] R. Bashyam and P. Zelenay, "A class of non-precious metal composite catalysts for fuel cells," *Nature*, vol. 443, no. 7107, pp. 63-66, 2006.
- [17] S. Chen, J. Duan, M. Jaroniec, and S. Z. Qiao, "Nitrogen and oxygen dual-doped carbon hydrogel film as a substrate-free electrode for highly efficient oxygen evolution reaction," *Advanced Materials*, vol. 26, no. 18, pp. 2925-2930, 2014.
- [18] E. Proietti *et al.*, "Iron-based cathode catalyst with enhanced power density in polymer electrolyte membrane fuel cells," *Nature communications*, vol. 2, no. 1, p. 416, 2011.
- [19] H. Wang, T. Maiyalagan, and X. Wang, "Review on recent progress in nitrogen-doped graphene: synthesis, characterization, and its potential applications," *AcS catalysis*, vol. 2, no. 5, pp. 781-794, 2012.
- [20] Y. Li *et al.*, "An oxygen reduction electrocatalyst based on carbon nanotube-graphene complexes," *Nature nanotechnology*, vol. 7, no. 6, pp. 394-400, 2012.
- [21] G. Wu, K. L. More, C. M. Johnston, and P. Zelenay, "High-performance electrocatalysts for oxygen reduction derived from polyaniline, iron, and cobalt," *Science*, vol. 332, no. 6028, pp. 443-447, 2011.
- [22] K. Gong, F. Du, Z. Xia, M. Durstock, and L. Dai, "Nitrogen-doped carbon nanotube arrays with high electrocatalytic activity for oxygen reduction," *science*, vol. 323, no. 5915, pp. 760-764, 2009.

- [23] L. Yu, H. B. Wu, and X. W. D. Lou, "Self-templated formation of hollow structures for electrochemical energy applications," *Accounts of chemical research*, vol. 50, no. 2, pp. 293-301, 2017.
- [24] Y. P. Zhu, C. Guo, Y. Zheng, and S.-Z. Qiao, "Surface and interface engineering of noble-metal-free electrocatalysts for efficient energy conversion processes," *Accounts of chemical research*, vol. 50, no. 4, pp. 915-923, 2017.
- [25] B. Li, H. M. Wen, Y. Cui, W. Zhou, G. Qian, and B. Chen, "Emerging multifunctional metal-organic framework materials," *Advanced Materials*, vol. 28, no. 40, pp. 8819-8860, 2016.
- [26] S. Bordiga, F. Bonino, K. P. Lillerud, and C. Lamberti, "X-ray absorption spectroscopies: useful tools to understand metallorganic frameworks structure and reactivity," *Chemical Society Reviews*, vol. 39, no. 12, pp. 4885-4927, 2010.
- [27] H. Zhang, G. Liu, L. Shi, H. Liu, T. Wang, and J. Ye, "Engineering coordination polymers for photocatalysis," *Nano energy*, vol. 22, pp. 149-168, 2016.
- [28] Y. V. Kaneti *et al.*, "Nanoarchitected design of porous materials and nanocomposites from metal-organic frameworks," *Advanced materials*, vol. 29, no. 12, p. 1604898, 2017.
- [29] P. Zhang, F. Sun, Z. Xiang, Z. Shen, J. Yun, and D. Cao, "ZIF-derived in situ nitrogen-doped porous carbons as efficient metal-free electrocatalysts for oxygen reduction reaction," *Energy & Environmental Science*, vol. 7, no. 1, pp. 442-450, 2014.
- [30] Q. Lin *et al.*, "New heterometallic zirconium metalloporphyrin frameworks and their heteroatom-activated high-surface-area carbon derivatives," *Journal of the American Chemical Society*, vol. 137, no. 6, pp. 2235-2238, 2015.
- [31] H. Furukawa, K. E. Cordova, M. O'Keeffe, and O. M. Yaghi, "The chemistry and applications of metal-organic frameworks," *Science*, vol. 341, no. 6149, p. 1230444, 2013.
- [32] H.-L. Jiang *et al.*, "From metal-organic framework to nanoporous carbon: toward a very high surface area and hydrogen uptake," *Journal of the American Chemical Society*, vol. 133, no. 31, pp. 11854-11857, 2011.
- [33] A. Aijaz, N. Fujiwara, and Q. Xu, "From metal-organic framework to nitrogen-decorated nanoporous carbons: high CO₂ uptake and efficient catalytic oxygen reduction," *Journal of the American Chemical Society*, vol. 136, no. 19, pp. 6790-6793, 2014.

- [34] Z. S. Wu *et al.*, "High-performance electrocatalysts for oxygen reduction derived from cobalt porphyrin-based conjugated mesoporous polymers," *Advanced materials*, vol. 26, no. 9, pp. 1450-1455, 2014.
- [35] W. Zhang, Z.-Y. Wu, H.-L. Jiang, and S.-H. Yu, "Nanowire-directed templating synthesis of metal–organic framework nanofibers and their derived porous doped carbon nanofibers for enhanced electrocatalysis," *Journal of the American Chemical Society*, vol. 136, no. 41, pp. 14385-14388, 2014.
- [36] P. Su *et al.*, "Nitrogen-doped carbon nanotubes derived from Zn–Fe-ZIF nanospheres and their application as efficient oxygen reduction electrocatalysts with in situ generated iron species," *Chemical Science*, vol. 4, no. 7, pp. 2941-2946, 2013.
- [37] J. R. Long and O. M. Yaghi, "The pervasive chemistry of metal–organic frameworks," *Chemical Society Reviews*, vol. 38, no. 5, pp. 1213-1214, 2009.
- [38] D. J. Tranchemontagne, J. L. Mendoza-Cortés, M. O'keeffe, and O. M. Yaghi, "Secondary building units, nets and bonding in the chemistry of metal–organic frameworks," *Chemical Society Reviews*, vol. 38, no. 5, pp. 1257-1283, 2009.
- [39] H. Zhang *et al.*, "Two enantiomeric 3D Zn (II)–carboxylate MOFs with double helical structures serving as a chiral source induced by hydrogen bonding," *CrystEngComm*, vol. 14, no. 12, pp. 4165-4167, 2012.
- [40] J.-K. Sun and Q. Xu, "Functional materials derived from open framework templates/precursors: synthesis and applications," *Energy & Environmental Science*, vol. 7, no. 7, pp. 2071-2100, 2014.
- [41] J. Tang *et al.*, "Cage-type highly graphitic porous carbon–Co₃O₄ polyhedron as the cathode of lithium–oxygen batteries," *ACS applied materials & interfaces*, vol. 8, no. 4, pp. 2796-2804, 2016.
- [42] P.-Q. Liao *et al.*, "Monodentate hydroxide as a super strong yet reversible active site for CO₂ capture from high-humidity flue gas," *Energy & Environmental Science*, vol. 8, no. 3, pp. 1011-1016, 2015.
- [43] N. L. Rosi *et al.*, "Hydrogen storage in microporous metal-organic frameworks," *Science*, vol. 300, no. 5622, pp. 1127-1129, 2003.

- [44] H. Furukawa *et al.*, "Ultra-high porosity in metal-organic frameworks," *Science*, vol. 329, no. 5990, pp. 424-428, 2010.
- [45] L. Wang and R. T. Yang, "New sorbents for hydrogen storage by hydrogen spillover—a review," *Energy & Environmental Science*, vol. 1, no. 2, pp. 268-279, 2008.
- [46] C. Wang, K. E. DeKrafft, and W. Lin, "Pt nanoparticles@ photoactive metal-organic frameworks: efficient hydrogen evolution via synergistic photoexcitation and electron injection," *Journal of the American Chemical Society*, vol. 134, no. 17, pp. 7211-7214, 2012.
- [47] Y. Horiuchi *et al.*, "Visible-light-promoted photocatalytic hydrogen production by using an amino-functionalized Ti (IV) metal-organic framework," *The Journal of Physical Chemistry C*, vol. 116, no. 39, pp. 20848-20853, 2012.
- [48] T. Zhou *et al.*, "Post-synthesis modification of a metal-organic framework to construct a bifunctional photocatalyst for hydrogen production," *Energy & Environmental Science*, vol. 6, no. 11, pp. 3229-3234, 2013.
- [49] Y.-P. Yuan, L.-S. Yin, S.-W. Cao, G.-S. Xu, C.-H. Li, and C. Xue, "Improving photocatalytic hydrogen production of metal-organic framework UiO-66 octahedrons by dye-sensitization," *Applied Catalysis B: Environmental*, vol. 168, pp. 572-576, 2015.
- [50] Z. Zhang, Z.-Z. Yao, S. Xiang, and B. Chen, "Perspective of microporous metal-organic frameworks for CO₂ capture and separation," *Energy & environmental science*, vol. 7, no. 9, pp. 2868-2899, 2014.
- [51] D. Britt, H. Furukawa, B. Wang, T. G. Glover, and O. M. Yaghi, "Highly efficient separation of carbon dioxide by a metal-organic framework replete with open metal sites," *Proceedings of the National Academy of Sciences*, vol. 106, no. 49, pp. 20637-20640, 2009.
- [52] H. Zhang *et al.*, "Surface-plasmon-enhanced photodriven CO₂ reduction catalyzed by metal-organic-framework-derived iron nanoparticles encapsulated by ultrathin carbon layers," *Advanced Materials*, vol. 28, no. 19, pp. 3703-3710, 2016.
- [53] P. Manna, J. Debgupta, S. Bose, and S. K. Das, "A mononuclear cobalt coordination complex locked in a confined space and acting as an electrochemical water-oxidation catalyst: A "ship-in-a-bottle" approach," *Angewandte Chemie*, vol. 128, no. 7, pp. 2471-2476, 2016.

- [54] B. Y. Xia, Y. Yan, N. Li, H. B. Wu, X. W. D. Lou, and X. Wang, "A metal–organic framework-derived bifunctional oxygen electrocatalyst," *Nature energy*, vol. 1, no. 1, pp. 1-8, 2016.
- [55] A. Aijaz *et al.*, "Co@ Co₃O₄ encapsulated in carbon nanotube-grafted nitrogen-doped carbon polyhedra as an advanced bifunctional oxygen electrode," *Angewandte Chemie International Edition*, vol. 55, no. 12, pp. 4087-4091, 2016.
- [56] T. Y. Ma, S. Dai, M. Jaroniec, and S. Z. Qiao, "Metal–organic framework derived hybrid Co₃O₄-carbon porous nanowire arrays as reversible oxygen evolution electrodes," *Journal of the American Chemical Society*, vol. 136, no. 39, pp. 13925-13931, 2014.
- [57] X.-Y. Yu, Y. Feng, B. Guan, X. W. D. Lou, and U. Paik, "Carbon coated porous nickel phosphides nanoplates for highly efficient oxygen evolution reaction," *Energy & Environmental Science*, vol. 9, no. 4, pp. 1246-1250, 2016.
- [58] P. He, X. Y. Yu, and X. W. Lou, "Carbon-incorporated nickel–cobalt mixed metal phosphide nanoboxes with enhanced electrocatalytic activity for oxygen evolution," *Angewandte Chemie International Edition*, vol. 56, no. 14, pp. 3897-3900, 2017.
- [59] B. Y. Guan, L. Yu, and X. W. Lou, "General synthesis of multishell mixed-metal oxyphosphide particles with enhanced electrocatalytic activity in the oxygen evolution reaction," *Angewandte Chemie International Edition*, vol. 56, no. 9, pp. 2386-2389, 2017.
- [60] A. Mahmood, W. Guo, H. Tabassum, and R. Zou, "Metal-organic framework-based nanomaterials for electrocatalysis," *Advanced Energy Materials*, vol. 6, no. 17, p. 1600423, 2016.
- [61] B. Y. Guan, L. Yu, and X. W. D. Lou, "A dual-metal–organic-framework derived electrocatalyst for oxygen reduction," *Energy & Environmental Science*, vol. 9, no. 10, pp. 3092-3096, 2016.
- [62] X. Y. Yu, L. Yu, and X. W. Lou, "Hollow nanostructures of molybdenum sulfides for electrochemical energy storage and conversion," *Small Methods*, vol. 1, no. 1-2, p. 1600020, 2017.
- [63] Y. M. Chen, X. Y. Yu, Z. Li, U. Paik, and X. W. Lou, "Hierarchical MoS₂ tubular structures internally wired by carbon nanotubes as a highly stable anode material for lithium-ion batteries," *Science advances*, vol. 2, no. 7, p. e1600021, 2016.

- [64] H. Hu, L. Han, M. Yu, Z. Wang, and X. W. D. Lou, "Metal–organic-framework-engaged formation of Co nanoparticle-embedded carbon@ Co₉S₈ double-shelled nanocages for efficient oxygen reduction," *Energy & Environmental Science*, vol. 9, no. 1, pp. 107-111, 2016.
- [65] Q. Li *et al.*, "Graphene/graphene-tube nanocomposites templated from cage-containing metal-organic frameworks for oxygen reduction in Li–O₂ batteries," *Advanced materials*, vol. 26, no. 9, pp. 1378-1386, 2014.
- [66] Y. Dou *et al.*, "Co₉S₈@ carbon porous nanocages derived from a metal–organic framework: a highly efficient bifunctional catalyst for aprotic Li–O₂ batteries," 2018.
- [67] W. Yin, Y. Shen, F. Zou, X. Hu, B. Chi, and Y. Huang, "Metal–organic framework derived ZnO/ZnFe₂O₄/C nanocages as stable cathode material for reversible lithium–oxygen batteries," *ACS applied materials & interfaces*, vol. 7, no. 8, pp. 4947-4954, 2015.
- [68] W. Chen *et al.*, "Hierarchical mesoporous γ -Fe₂O₃/carbon nanocomposites derived from metal organic frameworks as a cathode electrocatalyst for rechargeable Li-O₂ batteries," *Electrochimica Acta*, vol. 134, pp. 293-301, 2014.
- [69] J. Zhang *et al.*, "Porous cobalt–manganese oxide nanocubes derived from metal organic frameworks as a cathode catalyst for rechargeable Li–O₂ batteries," *Nanoscale*, vol. 7, no. 2, pp. 720-726, 2015.
- [70] Y.-C. Lu *et al.*, "Lithium–oxygen batteries: bridging mechanistic understanding and battery performance," *Energy & Environmental Science*, vol. 6, no. 3, pp. 750-768, 2013.
- [71] R. Zhao, Z. Liang, R. Zou, and Q. Xu, "Metal-organic frameworks for batteries," *Joule*, vol. 2, no. 11, pp. 2235-2259, 2018.
- [72] D. Wu *et al.*, "Metal–organic frameworks as cathode materials for Li–O₂ batteries," *Advanced Materials*, vol. 26, no. 20, pp. 3258-3262, 2014.
- [73] S. H. Kim, Y. J. Lee, D. H. Kim, and Y. J. Lee, "Bimetallic metal–organic frameworks as efficient cathode catalysts for Li–O₂ batteries," *ACS applied materials & interfaces*, vol. 10, no. 1, pp. 660-667, 2018.
- [74] W. Yan, Z. Guo, H. Xu, Y. Lou, J. Chen, and Q. Li, "Downsizing metal–organic frameworks with distinct morphologies as cathode materials for high-capacity Li–O₂ batteries," *Materials Chemistry Frontiers*, vol. 1, no. 7, pp. 1324-1330, 2017.

- [75] L. Cao *et al.*, "A high performance O₂ selective membrane based on CAU-1-NH₂@ polydopamine and the PMMA polymer for Li-air batteries," *Chemical Communications*, vol. 51, no. 21, pp. 4364-4367, 2015.
- [76] Y. Wu *et al.*, "A metal-organic framework-derived bifunctional catalyst for hybrid sodium-air batteries," *Applied Catalysis B: Environmental*, vol. 241, pp. 407-414, 2019.
- [77] J. Li, Y. Kang, D. Liu, Z. Lei, and P. Liu, "Nitrogen-doped graphitic carbon-supported ultrafine Co nanoparticles as an efficient multifunctional electrocatalyst for HER and rechargeable Zn-air batteries," *ACS applied materials & interfaces*, vol. 12, no. 5, pp. 5717-5729, 2020.
- [78] Y. Li, B. Jia, Y. Fan, K. Zhu, G. Li, and C. Y. Su, "Bimetallic zeolitic imidazolate framework derived carbon nanotubes embedded with Co nanoparticles for efficient bifunctional oxygen electrocatalyst," *Advanced Energy Materials*, vol. 8, no. 9, p. 1702048, 2018.
- [79] Z. Wang *et al.*, "Core-shell carbon materials derived from metal-organic frameworks as an efficient oxygen bifunctional electrocatalyst," *Nano Energy*, vol. 30, pp. 368-378, 2016.
- [80] H. Ning *et al.*, "Porous N-doped carbon-encapsulated CoNi alloy nanoparticles derived from MOFs as efficient bifunctional oxygen electrocatalysts," *ACS applied materials & interfaces*, vol. 11, no. 2, pp. 1957-1968, 2018.
- [81] A. Pendashteh *et al.*, "Bimetal zeolitic imidazolate framework (ZIF-9) derived nitrogen-doped porous carbon as efficient oxygen electrocatalysts for rechargeable Zn-air batteries," *Journal of Power Sources*, vol. 427, pp. 299-308, 2019.
- [82] D. Ding *et al.*, "Multi-level architecture optimization of MOF-templated Co-based nanoparticles embedded in hollow N-doped carbon polyhedra for efficient OER and ORR," *ACS Catalysis*, vol. 8, no. 9, pp. 7879-7888, 2018.
- [83] X. Li *et al.*, "ZIF-67-derived Co₃O₄@ carbon protected by oxygen-buffering CeO₂ as an efficient catalyst for boosting oxygen reduction/evolution reactions," *Journal of Materials Chemistry A*, vol. 7, no. 45, pp. 25853-25864, 2019.
- [84] R. Zhu, J. Ding, Y. Xu, J. Yang, Q. Xu, and H. Pang, " π -Conjugated molecule boosts metal-organic frameworks as efficient oxygen evolution reaction catalysts," *Small*, vol. 14, no. 50, p. 1803576, 2018.

- [85] M. Khalid, A. M. B. Honorato, H. Varela, and L. Dai, "Multifunctional electrocatalysts derived from conducting polymer and metal organic framework complexes," *Nano Energy*, vol. 45, pp. 127-135, 2018.
- [86] W. Wu, J. Liu, G. Chen, Y. Chen, and C. Xu, "Thin porous nanosheets of NiFe layered-double hydroxides toward a highly efficient electrocatalyst for water oxidation," *International Journal of Hydrogen Energy*, vol. 45, no. 3, pp. 1948-1958, 2020.
- [87] X. Guo, G. Liang, and A. Gu, "Designed formation of CoS₂ nanoboxes with enhanced oxygen evolution reaction electrocatalytic properties," *International Journal of Hydrogen Energy*, vol. 44, no. 59, pp. 31020-31028, 2019.
- [88] J. Xu, Y. Zhao, M. Li, G. Fan, L. Yang, and F. Li, "A strong coupled 2D metal-organic framework and ternary layered double hydroxide hierarchical nanocomposite as an excellent electrocatalyst for the oxygen evolution reaction," *Electrochimica Acta*, vol. 307, pp. 275-284, 2019.
- [89] D. Dong, Y. Liu, and J. Li, "Co₃O₄ hollow polyhedrons as bifunctional electrocatalysts for reduction and evolution reactions of oxygen," *Particle & Particle Systems Characterization*, vol. 33, no. 12, pp. 887-895, 2016.
- [90] S. Xun *et al.*, "MOF-derived cobalt oxides nanoparticles anchored on CoMoO₄ as a highly active electrocatalyst for oxygen evolution reaction," *Journal of Alloys and Compounds*, vol. 806, pp. 1097-1104, 2019.
- [91] H. Xu *et al.*, "MOF-derived hollow CoS decorated with CeO_x nanoparticles for boosting oxygen evolution reaction electrocatalysis," *Angewandte Chemie*, vol. 130, no. 28, pp. 8790-8794, 2018.
- [92] Z. Li *et al.*, "Facile preparation of CoSe₂ nano-vesicle derived from ZIF-67 and their application for efficient water oxidation," *Applied Surface Science*, vol. 504, p. 144368, 2020.
- [93] Q. Zha, W. Xu, X. Li, and Y. Ni, "Chlorine-doped α -Co (OH)₂ hollow nanododecahedrons prepared by a ZIF-67 self-sacrificing template route and enhanced OER catalytic activity," *Dalton Transactions*, vol. 48, no. 32, pp. 12127-12136, 2019.

- [94] Y. Wang, Y. Wang, L. Zhang, C.-S. Liu, and H. Pang, "Core-shell-type ZIF-8@ ZIF-67@ POM hybrids as efficient electrocatalysts for the oxygen evolution reaction," *Inorganic Chemistry Frontiers*, vol. 6, no. 9, pp. 2514-2520, 2019.
- [95] Y. Wang, M. Zhao, Q. Zhao, Q. Li, and H. Pang, "Facile synthesis of silver nanowire-zeolitic imidazolate framework 67 composites as high-performance bifunctional oxygen catalysts," *Nanoscale*, vol. 10, no. 33, pp. 15755-15762, 2018.
- [96] L. Li, T. Tian, J. Jiang, and L. Ai, "Hierarchically porous Co₃O₄ architectures with honeycomb-like structures for efficient oxygen generation from electrochemical water splitting," *Journal of Power Sources*, vol. 294, pp. 103-111, 2015.
- [97] L. Yang, D. Wang, Y. Lv, and D. Cao, "Nitrogen-doped graphitic carbons with encapsulated CoNi bimetallic nanoparticles as bifunctional electrocatalysts for rechargeable Zn-Air batteries," *Carbon*, vol. 144, pp. 8-14, 2019.
- [98] J. Wan, W. Chen, C. Chen, Q. Peng, D. Wang, and Y. Li, "Facile synthesis of CoNi_x nanoparticles embedded in nitrogen-carbon frameworks for highly efficient electrocatalytic oxygen evolution," *Chemical Communications*, vol. 53, no. 90, pp. 12177-12180, 2017.
- [99] X. Fu *et al.*, "Tailoring FeN₄ sites with edge enrichment for boosted oxygen reduction performance in proton exchange membrane fuel cell," *Advanced Energy Materials*, vol. 9, no. 11, p. 1803737, 2019.
- [100] L. Zhang, J. Xiao, H. Wang, and M. Shao, "Carbon-based electrocatalysts for hydrogen and oxygen evolution reactions," *Acs Catalysis*, vol. 7, no. 11, pp. 7855-7865, 2017.
- [101] H. Peng *et al.*, "Effect of transition metals on the structure and performance of the doped carbon catalysts derived from polyaniline and melamine for ORR application," *Acs Catalysis*, vol. 4, no. 10, pp. 3797-3805, 2014.
- [102] H. Khani, N. S. Grundish, D. O. Wipf, and J. B. Goodenough, "Graphitic-shell encapsulation of metal electrocatalysts for oxygen evolution, oxygen reduction, and hydrogen evolution in alkaline solution," *Advanced Energy Materials*, vol. 10, no. 1, p. 1903215, 2020.
- [103] H. Zou, G. Li, L. Duan, Z. Kou, and J. Wang, "In situ coupled amorphous cobalt nitride with nitrogen-doped graphene aerogel as a trifunctional electrocatalyst towards Zn-air

- battery derived full water splitting," *Applied Catalysis B: Environmental*, vol. 259, p. 118100, 2019.
- [104] W. Ye, Y. Yang, X. Fang, M. Arif, X. Chen, and D. Yan, "2D cocrystallized metal–organic nanosheet array as an efficient and stable bifunctional electrocatalyst for overall water splitting," *ACS Sustainable Chemistry & Engineering*, vol. 7, no. 21, pp. 18085-18092, 2019.
- [105] G. Fu *et al.*, "Boosting bifunctional oxygen electrocatalysis with 3D graphene aerogel-supported Ni/MnO particles," *Advanced Materials*, vol. 30, no. 5, p. 1704609, 2018.
- [106] A. Pendashteh, J. S. Sanchez, J. Palma, M. Anderson, and R. Marcilla, "Anchored NiCoMnS₄ nanoparticles on N-doped rGO: high-performance bifunctional electrocatalysts for rechargeable Zn-Air batteries," *Energy Storage Materials*, vol. 20, pp. 216-224, 2019.
- [107] T. Liu, F. Yang, G. Cheng, and W. Luo, "Reduced Graphene Oxide-Wrapped Co₉–xFe_xS₈/Co, Fe-N-C Composite as Bifunctional Electrocatalyst for Oxygen Reduction and Evolution," *Small*, vol. 14, no. 10, p. 1703748, 2018.
- [108] D. Zhou *et al.*, "Boosting oxygen reaction activity by coupling sulfides for high-performance rechargeable metal–air battery," *Journal of Materials Chemistry A*, vol. 6, no. 42, pp. 21162-21166, 2018.
- [109] Y. Li *et al.*, "N, S-Atom-coordinated Co₉S₈ ternary dopants within a porous graphene framework as efficient catalysts for oxygen reduction/evolution reactions," *Dalton Transactions*, vol. 47, no. 42, pp. 14992-15001, 2018.
- [110] S. Ghoshal *et al.*, "ZIF 67 based highly active electrocatalysts as oxygen electrodes in water electrolyzer," *ACS Applied Energy Materials*, vol. 2, no. 8, pp. 5568-5576, 2019.
- [111] B. J. Inkson, "Scanning electron microscopy (SEM) and transmission electron microscopy (TEM) for materials characterization," in *Materials characterization using nondestructive evaluation (NDE) methods*: Elsevier, 2016, pp. 17-43.
- [112] J. Epp, "X-ray diffraction (XRD) techniques for materials characterization," in *Materials characterization using nondestructive evaluation (NDE) methods*: Elsevier, 2016, pp. 81-124.
- [113] V. Țucureanu, A. Matei, and A. M. Avram, "FTIR spectroscopy for carbon family study," *Critical reviews in analytical chemistry*, vol. 46, no. 6, pp. 502-520, 2016.

- [114] R. Pilot, R. Signorini, C. Durante, L. Orian, M. Bhamidipati, and L. Fabris, "A review on surface-enhanced Raman scattering," *Biosensors*, vol. 9, no. 2, p. 57, 2019.
- [115] M. Tahir *et al.*, "Electrocatalytic oxygen evolution reaction for energy conversion and storage: a comprehensive review," *Nano Energy*, vol. 37, pp. 136-157, 2017.
- [116] Y.-L. Zhang *et al.*, "Advanced non-noble materials in bifunctional catalysts for ORR and OER toward aqueous metal–air batteries," *Nanoscale*, vol. 12, no. 42, pp. 21534-21559, 2020.
- [117] D. Kaewsai, S. Yeamdee, S. Supajaroon, and M. Hunsom, "ORR activity and stability of PtCr/C catalysts in a low temperature/pressure PEM fuel cell: Effect of heat treatment temperature," *International journal of hydrogen energy*, vol. 43, no. 10, pp. 5133-5144, 2018.
- [118] K. Cong, M. Ritter, S. Stumpf, B. Schröter, U. S. Schubert, and A. Ignaszak, "Metal-Free Electrocatalyst for Oxygen Reduction: Synthesis-Controlled Density of Catalytic Centers and Impact on ORR," *Electroanalysis*, vol. 26, no. 12, pp. 2567-2573, 2014.
- [119] Y. Chen *et al.*, "Utilizing in-situ polymerization of pyrrole to fabricate composited hollow nanospindles for boosting oxygen evolution reaction," *Applied Catalysis B: Environmental*, vol. 274, p. 119112, 2020.
- [120] B. J. Rani *et al.*, "In situ hydrothermal growth of SnS/Ni foam for electrochemical energy storage and conversion," *Materials Letters*, vol. 273, p. 127958, 2020.
- [121] T. Zhang, J. Du, H. Zhang, and C. Xu, "In-situ growth of ultrathin ZIF-67 nanosheets on conductive Ti@ TiO₂/CdS substrate for high-efficient electrochemical catalysis," *Electrochimica Acta*, vol. 219, pp. 623-629, 2016.
- [122] A. Hosseini, A. Amjad, R. Hosseinzadeh-Khanmiri, E. Ghorbani-Kalhor, M. Babazadeh, and E. Vessally, "Nanocomposite of ZIF-67 metal–organic framework with reduced graphene oxide nanosheets for high-performance supercapacitor applications," *Journal of Materials Science: Materials in Electronics*, vol. 28, pp. 18040-18048, 2017.
- [123] Z. Wang *et al.*, "Electrochemical performance and transformation of Co-MOF/reduced graphene oxide composite," *Materials Letters*, vol. 193, pp. 216-219, 2017.
- [124] J. Qian, F. Sun, and L. Qin, "Hydrothermal synthesis of zeolitic imidazolate framework-67 (ZIF-67) nanocrystals," *Materials Letters*, vol. 82, pp. 220-223, 2012.

- [125] Q. Wang *et al.*, "ZIF-67 derived amorphous CoNi₂S₄ nanocages with nanosheet arrays on the shell for a high-performance asymmetric supercapacitor," *Chemical Engineering Journal*, vol. 327, pp. 387-396, 2017.
- [126] W. Zhang *et al.*, "Nanocomposites of zeolitic imidazolate frameworks on graphene oxide for pseudocapacitor applications," *Journal of Applied Electrochemistry*, vol. 46, pp. 441-450, 2016.
- [127] N. Mironova-Ulmane *et al.*, "Synthesis and vibration spectroscopy of nano-sized manganese oxides," 2018.
- [128] A. Indra, P. W. Menezes, F. Schuster, and M. Driess, "Significant role of Mn (III) sites in eg₁ configuration in manganese oxide catalysts for efficient artificial water oxidation," *Journal of Photochemistry and Photobiology B: Biology*, vol. 152, pp. 156-161, 2015.
- [129] Z. Jiang, K. Huang, D. Yang, S. Wang, H. Zhong, and C. Jiang, "Facile preparation of Mn₃O₄ hollow microspheres via reduction of pentachloropyridine and their performance in lithium-ion batteries," *RSC advances*, vol. 7, no. 14, pp. 8264-8271, 2017.
- [130] Q. Zhou, B. Jin, P. Zhao, S. Chu, and R. Peng, "rGO/CNQDs/ZIF-67 composite aerogel for efficient extraction of uranium in wastewater," *Chemical Engineering Journal*, vol. 419, p. 129622, 2021.
- [131] S. Sundriyal, H. Kaur, S. K. Bhardwaj, S. Mishra, K.-H. Kim, and A. Deep, "Metal-organic frameworks and their composites as efficient electrodes for supercapacitor applications," *Coordination Chemistry Reviews*, vol. 369, pp. 15-38, 2018.
- [132] D. C. Marcano *et al.*, "Improved synthesis of graphene oxide," *ACS nano*, vol. 4, no. 8, pp. 4806-4814, 2010.
- [133] F. Zhang, L. Hao, L. Zhang, and X. Zhang, "Solid-state thermolysis preparation of Co₃O₄ nano/micro superstructures from metal-organic framework for supercapacitors," *Int. J. Electrochem. Sci*, vol. 6, pp. 2943-2954, 2011.
- [134] S. Sundriyal, V. Shrivastav, H. Kaur, S. Mishra, and A. Deep, "High-performance symmetrical supercapacitor with a combination of a ZIF-67/rGO composite electrode and a redox additive electrolyte," *ACS omega*, vol. 3, no. 12, pp. 17348-17358, 2018.

- [135] D. Zhang *et al.*, "Quick synthesis of zeolitic imidazolate framework microflowers with enhanced supercapacitor and electrocatalytic performances," *RSC advances*, vol. 5, no. 72, pp. 58772-58776, 2015.
- [136] F. Wang *et al.*, "Core-shell-structured Co@ Co₄N nanoparticles encapsulated into MnO-modified porous N-doping carbon nanocubes as bifunctional catalysts for rechargeable Zn-air batteries," *Journal of Energy Chemistry*, vol. 50, pp. 52-62, 2020.
- [137] L. Jiao, Y.-X. Zhou, and H.-L. Jiang, "Metal-organic framework-based CoP/reduced graphene oxide: high-performance bifunctional electrocatalyst for overall water splitting," *Chemical Science*, vol. 7, no. 3, pp. 1690-1695, 2016.
- [138] Q. Li *et al.*, "Metal-organic framework-derived bamboo-like nitrogen-doped graphene tubes as an active matrix for hybrid oxygen-reduction electrocatalysts," vol. 11, no. 12, pp. 1443-1452, 2015.
- [139] A. Sumboja *et al.*, "Manganese oxide catalyst grown on carbon paper as an air cathode for high-performance rechargeable zinc-air batteries," *ChemPlusChem*, vol. 80, no. 8, pp. 1341-1346, 2015.
- [140] K. J. Vetter, *Electrochemical kinetics: theoretical aspects*. Elsevier, 2013.
- [141] N. E. A. Shuhaimi, L. P. Teo, H. J. Woo, S. R. Majid, and A. K. Arof, "Electrical double-layer capacitors with plasticized polymer electrolyte based on methyl cellulose," *Polymer bulletin*, vol. 69, pp. 807-826, 2012.
- [142] U. A. Asif, T. Noor, E. Pervaiz, N. Iqbal, and N. Zaman, "LSTN (La_{0.4}Sr_{0.4}Ti_{0.9}Ni_{0.1}O₃-&) perovskite and graphitic carbon nitride (g-C₃N₄) hybrids as a bifunctional electrocatalyst for water-splitting applications," *Journal of Alloys and Compounds*, p. 168668, 2023.
- [143] Y.-P. Gao, K.-J. Huang, X. Wu, Z.-Q. Hou, and Y.-Y. Liu, "MoS₂ nanosheets assembling three-dimensional nanospheres for enhanced-performance supercapacitor," *Journal of alloys and compounds*, vol. 741, pp. 174-181, 2018.
- [144] X. Zhang *et al.*, "Synergistic effects of lanthanum and strontium to enhance the osteogenic activity of TiO₂ nanotube biological interface," *Ceramics International*, vol. 46, no. 9, pp. 13969-13979, 2020.

- [145] W. Zhang, Y. Tan, Y. Gao, J. Wu, and B. Tang, "Synthesis of amorphous cobalt-boron alloy/highly ordered mesoporous carbon nanofiber arrays as advanced pseudocapacitor material," *Journal of Solid State Electrochemistry*, vol. 19, pp. 593-598, 2015.